



This is an author manuscript post-peer-reviewing (accepted version) of the original publication. The layout of the published version may differ .

---

## A Holocene record of snow-avalanche and flood activity reconstructed from a lacustrine sedimentary sequence in Oldevatnet, western Norway

---

Vasskog, K.; Nesje, A.; Storen, E. N.; Waldmann, Nicolas; Chapron, Emmanuel; Ariztegui, Daniel

### How to cite

VASSKOG, K. et al. A Holocene record of snow-avalanche and flood activity reconstructed from a lacustrine sedimentary sequence in Oldevatnet, western Norway. In: Holocene, 2011, vol. 21, n° 4, p. 597–614. doi: 10.1177/0959683610391316

This publication URL: <https://archive-ouverte.unige.ch/unige:17078>

Publication DOI: [10.1177/0959683610391316](https://doi.org/10.1177/0959683610391316)

**A Holocene record of snow-avalanche and flood activity reconstructed from a lacustrine sedimentary sequence in Oldevatnet, western Norway**

Kristian Vasskog, Atle Nesje, Eivind Nagel Støren, Nicolas Waldmann, Emmanuel Chapron and Daniel Ariztegui

*The Holocene* published online 22 February 2011

DOI: 10.1177/0959683610391316

The online version of this article can be found at:

<http://hol.sagepub.com/content/early/2011/02/19/0959683610391316>

---

Published by:



<http://www.sagepublications.com>

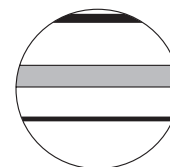
**Additional services and information for *The Holocene* can be found at:**

**Email Alerts:** <http://hol.sagepub.com/cgi/alerts>


**Subscriptions:** <http://hol.sagepub.com/subscriptions>

**Reprints:** <http://www.sagepub.com/journalsReprints.nav>

**Permissions:** <http://www.sagepub.com/journalsPermissions.nav>



# A Holocene record of snow-avalanche and flood activity reconstructed from a lacustrine sedimentary sequence in Oldevatnet, western Norway

The Holocene  
1–18  
© The Author(s) 2011  
Reprints and permission:  
sagepub.co.uk/journalsPermissions.nav  
DOI: 10.1177/0959683610391316  
hol.sagepub.com  


Kristian Vasskog,<sup>1,2</sup> Atle Nesje,<sup>1,2</sup> Eivind Nagel Støren,<sup>1,2</sup>  
Nicolas Waldmann,<sup>1,3</sup> Emmanuel Chapron<sup>4</sup> and Daniel Ariztegui<sup>3</sup>

## Abstract

Two lacustrine sediment cores from Oldevatnet in western Norway have been studied in order to produce a record of floods, mass-wasting events and glacier fluctuations during the last 7300 years. River floods, density currents and snow-avalanches have deposited distinct 'event layers' at the lake floor throughout this time interval. In this study, a novel approach has been applied to distinguish event layers from the continuous background sedimentation, using Rb/Sr-ratios from X-Ray Fluorescence data. Grain-size distribution and the sedimentological parameters 'mean' and 'sorting' were used to further infer the depositional processes behind each layer. Our data suggest a record dominated by snow-avalanches, with the largest activity occurring during the 'Little Ice Age' (LIA). This increase in snow-avalanche activity observed during the LIA was probably caused by a combination of generally increasing winter precipitation and the advance of local glaciers towards the steep valley sides. Several fluctuations in snow-avalanche activity are also recognized prior to the LIA. Proxies of glacial activity from the background sediments indicate a similar development as earlier palaeoclimatic reconstructions from the area. It differs from previous reconstructions, however, by suggesting a lower glacial activity in the period from 2200 to 1000 cal. yr BP.

## Keywords

density currents, floods, Holocene, palaeoclimate, proglacial lake sediments, snow-avalanches, western Norway

## Introduction

Extreme weather and related mass-wasting events are expected to become more frequent in the future because of global climate change (Intergovernmental Panel on Climate Change (IPCC), 2007; Palmer and Räisänen, 2002). In western Norway, instrumental data show an increase in both extreme 24-hour precipitation events and annual mean precipitation during the last 100 years (Alfsnes and Førland, 2006; Førland et al., 2007; Hanssen-Bauer, 2005). This trend is expected to continue towards the end of the twenty-first century (Benestad, 2007; Førland et al., 2007; Iversen et al., 2005), although no significant increase in related mass-wasting activity is envisaged (Hanssen-Bauer et al., 2009; Kronholm and Stalsberg, 2009). Analysis of historical data from the same region shows a significant relationship between extreme weather events and mass-wasting activity, with ~24-hour extreme precipitation events being the most important triggering factor for both snow-avalanches and debris-flows (Førland et al., 2007). However, to study the long-term relationship between climate and mass-wasting, prehistoric records are needed. An increasing number of Holocene mass-wasting and flood records are now becoming available from southern Norway (e.g. Blikra and Nesje, 1997; Blikra and Selvik, 1998; Bøe et al., 2006; Matthews et al., 2009; Nesje et al., 2001a, 2007; Sletten and Blikra, 2007; Sletten et al., 2003; Støren et al., 2008). Lake sediments are considered to be one of the best high-resolution terrestrial archives of Holocene climate change in Scandinavia, and Norwegian

proglacial lakes have been studied extensively to reconstruct past glacier variability and climate change (e.g. Bakke et al. 2005a, b, c; Lie et al., 2004; Matthews and Karlén, 1992; Matthews et al., 2000; Nesje et al., 2000, 2001b; Shakesby et al., 2007; Svendsen and Mangerud, 1997). Sediment layers deposited by mass-wasting and flood events have a high preservation potential in lacustrine sequences, as they are usually covered by continuous sedimentation in a relatively short period of time. In this study we present a record of Holocene mass-wasting and flood events from western Norway, reconstructed from lake sediment cores and seismic profiling. Such data contribute to an increased understanding of the relationship between climate and mass-wasting activity, something that is essential in order to assess the full impact of future climate change.

<sup>1</sup>University of Bergen, Norway

<sup>2</sup>Bjerknes Centre for Climate Research, Norway

<sup>3</sup>University of Geneva, Switzerland

<sup>4</sup>Université d'Orléans, France

Received 30 March 2010; revised manuscript accepted 9 September 2010

## Corresponding author:

Kristian Vasskog, Bjerknes Centre for Climate Research, Allégt. 55,  
N-5007, Norway

Email: kristian.vasskog@uni.no



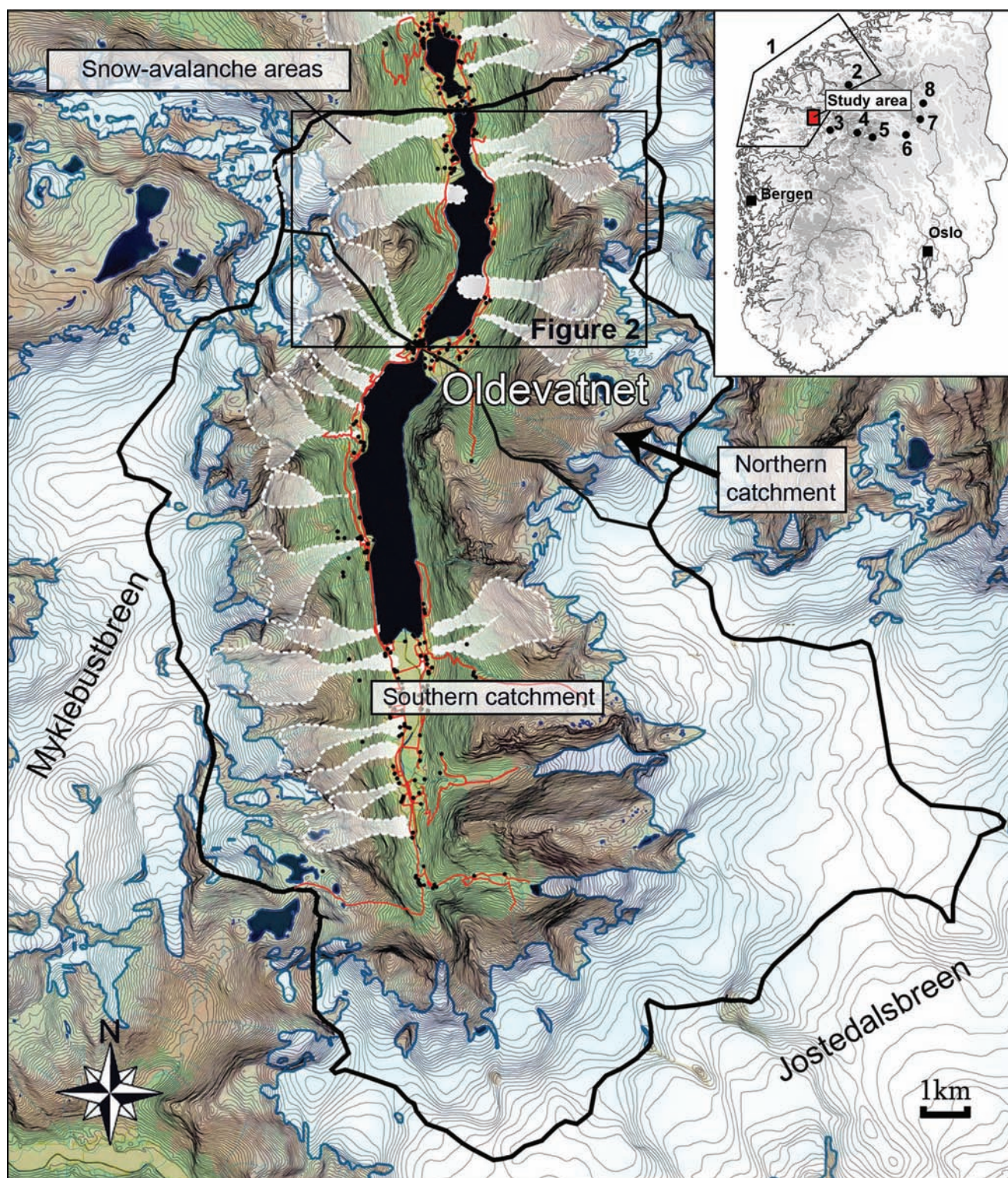


**Figure 1.** Map including Oldevatnet and the two catchment areas, shown with 20 m contour lines. Areas where damaging snow-avalanches have been recorded are shaded white, roads are marked red and buildings are black dots. Inset map of southern Norway shows the location of the study area (red) and other localities discussed in the text: 1, the Møre area that contains numerous localities (see Blikra and Nesje, 1997 and Blikra and Selvik, 1998 for all localities); 2, Ulvådalvatnet (Sletten et al., 2003); 3, Vanndalsvatnet (Nesje et al., 2007); 4, Leirdalen (Matthews et al., 2009); 5, Russvatnet (Støren et al., 2008); 6, The Otta area (Sletten and Blikra, 2007); 7, Atnsjøen (Nesje et al., 2001a); 8, Butjønna (Bøe et al., 2006)

## Study site

Oldevatnet ( $c. 8 \text{ km}^2$ ) is situated in Oldedalen, a tributary valley branching off southwards from the innermost part of Nordfjorden in western Norway (Figure 1). The lake is divided into two main basins connected by a narrow channel. Oldedalen is presently surrounded by the Jostedalsbreen glacier in the south and

east, and the Myklebustbreen glacier in the west, leaving about half of the  $c. 180 \text{ km}^2$  total catchment area covered by glaciers. These two major glaciers contribute with large amounts of glacial meltwater to the southern lake basin, whereas the northern basin receives meltwater mainly from smaller, local glaciers. The outer limit of the Younger Dryas (YD) glaciation was situated at Nordfjordeid, approximately 40 km west of Oldevatnet, whereas



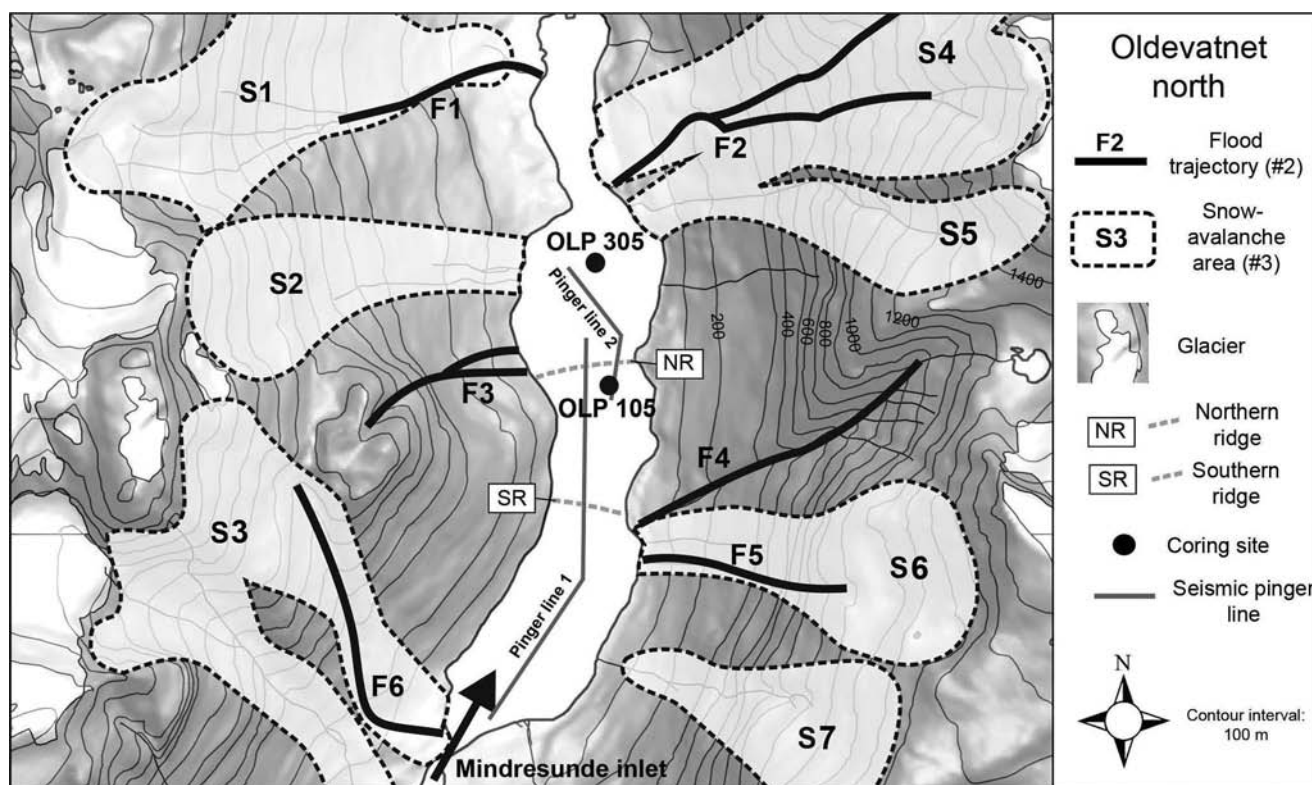


**Figure 2.** Map showing the northern Oldevatnet basin. Coring sites are marked with black circles. Grey lines indicate seismic Pinger profiles shown in Figure 3. Snow-avalanche areas and flood trajectories are named S1–S7 and F1–F6, respectively, and represent areas where at least one damaging event has been recorded

YD marginal moraines are located at about 1000 m a.s.l. in Olden (Rye et al., 1997). Deglaciation occurred rapidly during the Pre-boreal, leaving the basin now occupied by Oldevatnet as part of the fjord due to the large glacio-isostatic depression at the time. Sediments in the basal part of the OLP 105 core that is presented in this study were confirmed to be of marine origin by a preliminary investigation of microscopic algae (for methodology see: Kaland, 1984; Vasskog, 2006). Age–depth calculations for the core (see Discussion) indicate that Oldevatnet was isolated from the sea sometime before 7300 cal. yr BP. This is in agreement with shoreline diagrams from Sunnmøre and Sør-Trøndelag (Svendsen and Mangerud, 1987). Bedrock within the catchment area is relatively uniform, consisting mostly of granitic and diorite gneisses, quartz monzonite and small patches of granite (Lutro and Tveten, 1996). The steep valley sides surrounding Oldevatnet rise from the lake surface at 33 m a.s.l. to more than 1500 m a.s.l., leaving the area vulnerable to hazardous slope processes. At present snow-avalanches occur at a near annual rate, whereas several damaging rock falls and flood-induced debris-flows have been recorded historically (Nesje and Aa, 1989). Historical data on damaging mass-wasting events in this area extends back to around AD 1620 (online data base at [www.skrednett.no](http://www.skrednett.no)). The historical data show that large snow-avalanches occur in the east-facing slopes after periods of westerly winds (areas S1–S3 in Figure 2), and in the west-facing slopes following northerly or easterly winds (areas S4–S7 in Figure 2) (Nesje and Aa, 1989). Furthermore, it has been documented that deposits from large snow-avalanches are able to reach the lake. In the east-facing S2 avalanche area at Beinnes (Figure 2), snow-avalanches have created waves large enough to damage buildings at the opposite side of the lake (Nesje and Aa, 1989). In the west-facing S6 avalanche

area a particularly dramatic event occurred at 8 March 1949 when a large snow-avalanche crossed the entire lake and ascended 400–500 m up into the opposing valley side, crushing the lake ice and causing two casualties (Nesje and Aa, 1989).

## Methods

A seismic survey was accomplished in Oldevatnet, collecting single-channel, high-resolution seismic data (3.5 kHz pinger source) (Figure 3), digitally recorded in SEG-Y format with an Octopus acquisition unit, using a non-differential global positioning system (GPS) with an average accuracy of  $\pm 5$  m. Pinger data were processed by band pass filtering (2–6 kHz) and gaining with Automatic Gain Control (AGC; window length 100 ms). Constant shallow noise was digitally removed and a water bottom mute applied. The seismic data were interpreted using the Kingdom Suite™ software (Seismic Micro-Technology Inc). For calculation of velocity, an average of 1470 m/s and 1500 m/s was assumed for the water column and the sedimentary infill, respectively. Based on the interpretation of the seismic data, two sediment cores were retrieved from the northern Oldevatnet basin at ~40 m water depth (Figures 2 and 3), using a modified piston corer (Nesje, 1992) from a coring platform. The 4.0 m long OLP 305 core was collected close to a colluvial fan to capture proximal mass-wasting events whereas the 4.8 m long OLP 105 core was retrieved ~700 m further south, to better capture a long-term climate signal with minimal disturbing influence from mass-wasting events. Following fieldwork the cores were split lengthwise, with one of the halves being archived for future reference while the other halves were photographed, described and prepared for further analysis. The cores were first measured for

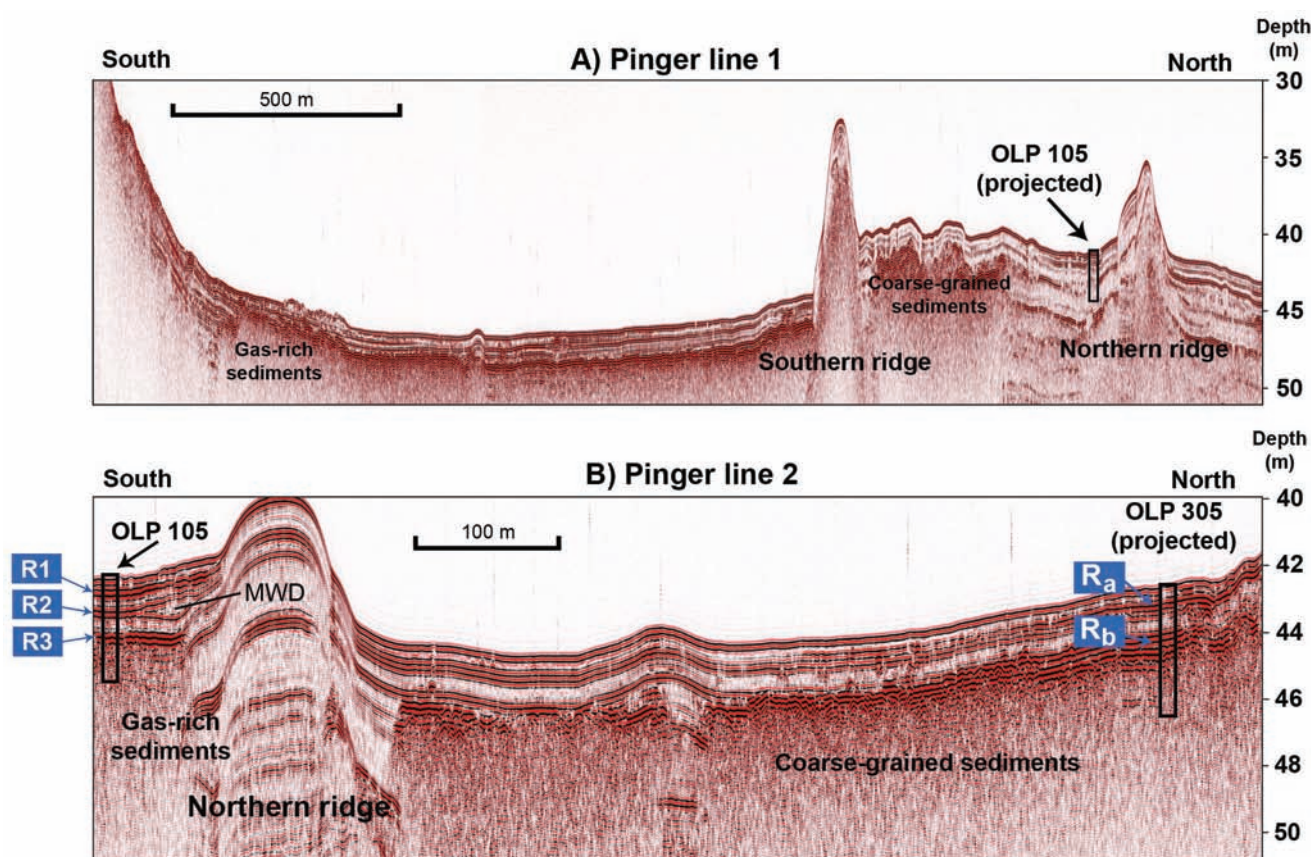


**Figure 3.** 3.5 kHz Pinger profiles 1 (A) and 2 (B) from the northern Oldevatnet basin (see Figure 2 for location). Significant seismic reflectors at the OLP 105 and OLP 305 sites are marked R1–R3 and  $R_a$ – $R_b$ , respectively. Note the different depth and horizontal scales between (A) and (B). Sediments displaying seismic signatures of mass-wasting deposits are labelled MWD

magnetic susceptibility (MS) using a Bartington MS2 point sensor. Sediment samples of 1 cm<sup>3</sup> were extracted at 0.5 cm intervals, dried overnight at 105°C and weighed for dry bulk density (DBD) (Bakke et al., 2005a, b). The samples were then ignited for 1 h at 550°C, cooled to room temperature in a desiccator, and weighed again for loss-on-ignition (LOI) (Dean, 1974). Samples for grain-size analysis were extracted continuously every centimetre throughout the OLP 105 core, and wet-sieved at 1 mm and 125 µm, before analyzing the <125 µm fraction in a Micromeritics SediGraph 5100 (measurement window set from 1 to 125 µm) in combination with a MasterTech 5.1 automatic sampling device. Grain-size statistics were extracted from the SediGraph data using the GRADISTAT software (Blott and Pye, 2001).

Core OLP 105 was further analyzed using an ITRAX, X-Ray Fluorescence (XRF) core scanner, employing a Cr x-ray tube (Croudace et al., 2006) at a resolution of 500 µm. To establish a chronology for the cores, 15 samples of plant macrofossils were extracted and <sup>14</sup>C AMS dated at the Poznan Radiocarbon Laboratory (Table 1). The ‘NORPEC sampling protocol for AMS radiocarbon dating’ (Birks and Lotter, 2000) was followed for macrofossil extraction. All ages were calibrated using the online OxCal v4.1.3 software (Bronk-Ramsey, 2009) with the IntCal04 terrestrial calibration curve (Reimer et al., 2004).

## Results

### Seismic profiling

The 3.5 kHz seismic profiles are characterized by limited acoustic penetration (between 10 and 2 m below the lake floor),

and feature a few continuous high-amplitude reflections with a draping geometry (Figure 3). Two subaquatic ridges in the northern part of the basin (possibly recessional moraines) make up a smaller sub-basin where similar high-amplitude reflections are locally developed. At the foot of slopes connected to the lake shore and the subaquatic ridges, several lens-shaped bodies are identified with chaotic internal reflections or transparent acoustic facies, features that are typical of mass-wasting deposits (MWDs, Figure 3). Core OLP 105 and OLP 305 were thus retrieved from two different sub-basins separated by the northern subaquatic ridge in close proximity to MWDs, making it possible to identify the nature of several seismic reflections (labelled R1, R2, R3,  $R_a$  and  $R_b$  in Figure 3 and Figure 4) and sediment with no acoustic penetration.

### Core stratigraphy

Visual inspection of the cores from Oldevatnet shows an olive-grey, fine-grained sediment (background sediment) interspersed with coarse-grained, brown units which are usually rich in terrestrial plant macrofossils (event layers) (Figure 4). In core OLP 105 the background sediment dominates, whereas in OLP 305 event layers constitute more than half of the core. Event layers have a generally higher organic content than the background sediment (Figure 4), and results of the XRF analysis show that they also feature a consistently lower ratio of rubidium ( $R_b$ ) to strontium (Sr) than the background sediment (Figure 5). The significance of this geochemical difference is treated in the Discussion section below. Based on a closer analysis of grain-size data the



**Table 1.**  $^{14}\text{C}$  dates and calibrated ages from core OLP 105 and OLP 305

Date	Core	Depth (cm)	Material	Weight (mg)	$^{14}\text{C}$ -age (BP)	Calibrated age BP ( $2\sigma$ )	Weighted mean	Cal. yr BP AD 2000
Poz-21750	OLP 105	9–10	Moss (unidentified)	3.5	60 $\pm$ 30	258–31	120	170
Poz-21751	OLP 105	58–60	<i>Betula</i> sp. fruits. <i>Betula</i> sp. catkin scales	4.3	540 $\pm$ 30	634–513	560	610
Poz-21752	OLP 105	140–142	<i>Betula</i> sp. fruits. <i>Betula</i> sp. catkin scales. leaf fragment of <i>Betula</i> sp. or <i>Salix</i> sp.	3.0	1900 $\pm$ 30	1923–1737	1840	1890
Poz-21753	OLP 105	199–200	<i>Betula</i> sp. fruits. leaf fragment of <i>Betula</i> sp. or <i>Salix</i> sp. and cone scale of <i>Pinus</i> sp.	2.7	2690 $\pm$ 35	2855–2750	2800	2850
Poz-21754	OLP 105	264–265	<i>Sorbus</i> sp. seeds. leaf fragments of <i>Betula</i> sp. or <i>Salix</i> sp.	4.3	4005 $\pm$ 35	4569–4414	4480	4530
Poz-21755	OLP 105	318–319	<i>Betula</i> sp. fruits. leaf fragment of <i>Betula</i> sp. or <i>Salix</i> sp.	3.0	5350 $\pm$ 40	6273–6000	6130	6180
Poz-21756	OLP 105	340–341	<i>Betula</i> sp. fruits. <i>Betula</i> sp. catkin scales. small twigs with bark	25.1	6280 $\pm$ 40	7309–7029	7210	7260
Poz-21757	OLP 305	25–26	<i>Betula</i> sp. fruits. catkin scales and leaf fragments. terrestrial moss ( <i>Racomitrium</i> sp.)	8.2	145 $\pm$ 30	283–2	150	200
Poz-21758	OLP 305	176–177	<i>Betula</i> sp. twig. <i>Salix</i> sp. bark	5.6	1260 $\pm$ 30	1281–1088	1210	1260
Poz-26483	OLP 305	245–246	<i>Betula</i> sp. fruits. leaf fragments. bark ( <i>Betula</i> sp. or <i>Salix</i> sp.)	3.8	2680 $\pm$ 35	2850–2748	2790	2840
Poz-26484	OLP 305	295–296	<i>Betula nana</i> fruit. <i>Betula</i> sp. fruits. catkin scales and leaf fragments	3.5	2200 $\pm$ 35	2326–2131	2230	2280
Poz-26485	OLP 305	325–326	<i>Betula</i> sp. fruits. catkin scales and leaf fragments. small twig with bark	12.6	2525 $\pm$ 35	2745–2487	2550	2600
Poz-26487	OLP 305	342–343	<i>Betula</i> sp. fruits and catkin scale fragment. <i>Betula</i> sp. or <i>Salix</i> sp. twig with bark	11.0	2510 $\pm$ 35	2740–2468	2620	2670
Poz-26488	OLP 305	362–364	<i>Betula</i> sp. fruits and catkin scales	3.0	2530 $\pm$ 35	2747–2488	2710	2760
Poz-21760	OLP 305	393–394	Leaf fragments of <i>Betula</i> sp. or <i>Salix</i> sp.	3.2	2985 $\pm$ 35	3326–3040	3170	3220

event layers are further classified into three different unit types named F-, S- and D-units (Figure 6), which are interpreted as flood-, snow-avalanche- and density current deposits, respectively (see Discussion). S-units (snow-avalanche deposits) are by far the most abundant unit type, comprising 47 of the total 61 event layers, whereas twelve F-units and two D-units are recognized. The different units are more closely described below following Blott and Pye (2001) sediment nomenclature. Note that a high sorting value reflects poorly sorted sediment whereas a low sorting value reflects well-sorted sediment. Unit descriptions refer to core OLP 105.

**Background sedimentation.** The background sediment consists of an olive-grey, highly minerogenic, fine to very fine silt. LOI values range between 2 and 6% throughout the core, whereas clay content is high, ranging from about 40 to 60% in weight. Sorting is relatively poor with very sparse content of plant macrofossils. Average grain-size and sorting values of the background sediment for the entire core are 4.85  $\mu\text{m}$  and 2.78  $\mu\text{m}$ , respectively. The coefficient of determination ( $R^2$ ) between mean and sorting values is 0.63, with a positive correlation of  $r = 0.79$ . The SediGraph samples (1–125  $\mu\text{m}$ ) generally show a bimodal grain-size distribution with the main modes being clay to very fine silt, and medium to coarse silt.

**F-units.** The F-units comprise easily distinguishable brown layers featuring a high content of terrestrial plant macrofossils and relatively well-sorted, coarse-grained minerogenic particles (Figure 6). While the actual sorting values are within the same range as in the background sediment, the F-units feature a higher degree of sorting relative to grain-size. This can be expressed by the average mean/sorting ratio, which is 2.44 for F-units,

compared with 1.74 for the background sediment. Some of the layers feature a gradual upper limit, where the organic material is fining-upwards and finally disappearing. Because of the high content of macrofossils, LOI values are usually higher when compared with the background sediment, whereas DBD and MS values are usually lower. In the grain-size distributions, F-units show a single dominant mode in the coarse silt fraction (Figure 6).

**S-units.** S-units display a poorer sorting than the F-units and feature scattered grains >1 mm (Figure 6). The SediGraph data do not include grains >125  $\mu\text{m}$ , meaning that the true sorting value of layers containing grains >1 mm are much poorer than the values suggested by the SediGraph data alone. Grains of up to 6 mm in diameter were registered in the S-units, whereas in the other unit types no grains >125  $\mu\text{m}$  were detected. A closer inspection of the grain-size distributions reveals that the S-units are strongly polymodal, which explains the low sorting value and further distinguish S-units from F-units.

**D-units.** D-units display a clear normal grading and are distinguished from the other units by exceptionally high mean grain-sizes combined with low sorting values (Figure 6). Organic content is low in the basal part and increases towards the top of the units. Some of this is attributed to terrestrial macrofossils. Only two D-units are recognized throughout core OLP 105.

## Discussion

The primary objective of the core analysis was to distinguish rapid, periodic sedimentation, such as floods, mass-wasting events or density current deposits from the continuous background sedimentation, and thus reconstruct a chronology of

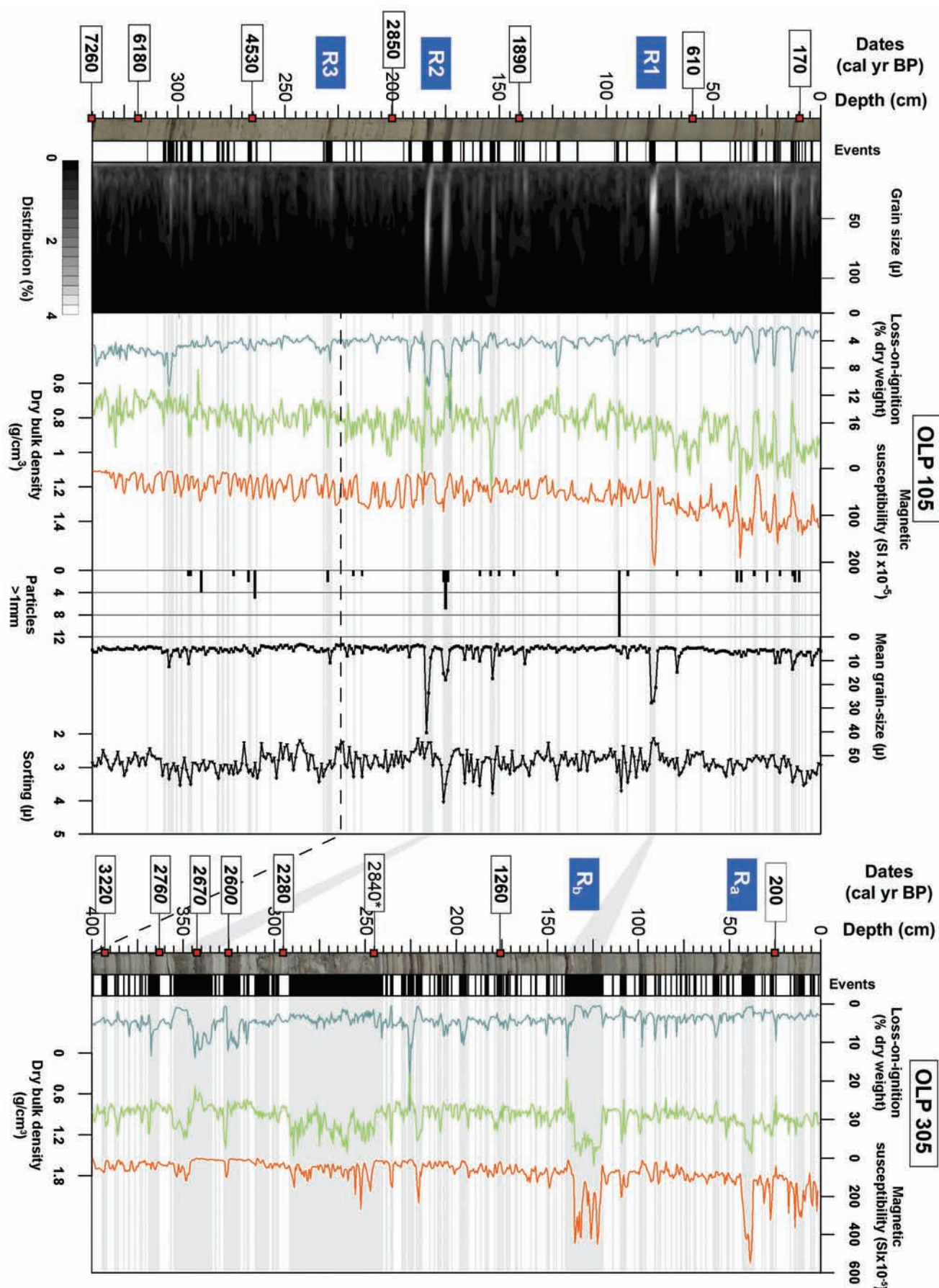


**Figure 4.** Data from cores OLP 105 and OLP 305. Loss-on-ignition, dry bulk density and magnetic susceptibility are shown for both cores. Mean grain-size, sorting and number of grains >1 mm are shown for OLP 105 in addition to a surface plot of the grain-size data (Beierle et al., 2002). Sediments interpreted to have been deposited by mass-wasting events are shown as black bars to the right of the photographs and shaded grey behind the data. Dates are given as cal. yr BP (AD 2000). The age marked with \* is interpreted as redeposited and thereby rejected. Ages in *italic* fall into a 'plateau' in the  $^{14}\text{C}$  calibration curve (see text and Figure 7). Positions of seismic reflectors shown in Figure 3 are indicated (R1–R3 and  $R_a$ – $R_b$ )



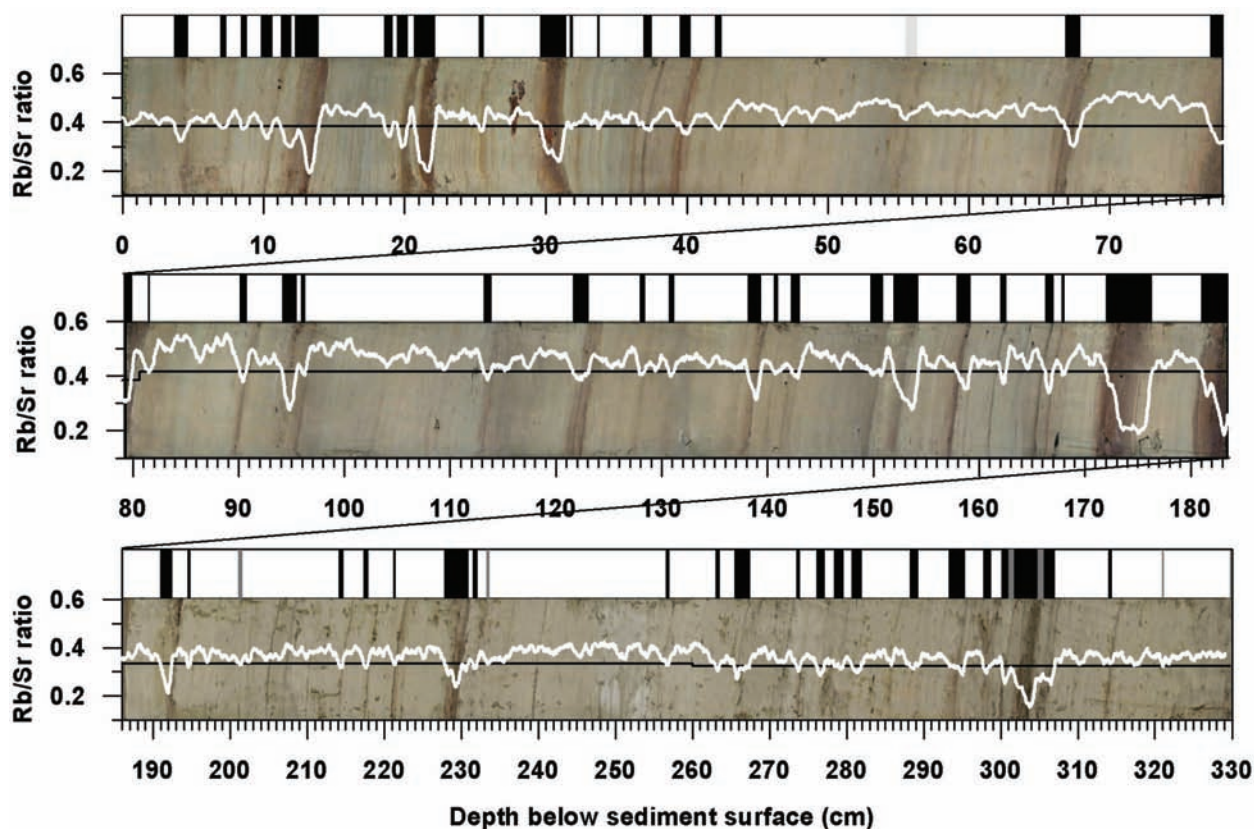


**Figure 5.** Photographs of the upper three core sections of OLP 105 showing an 11-point running mean of the Rb/Sr-ratio as a white line. Intervals displaying Rb/Sr-ratios below the twentieth percentile of each core section (black line) are interpreted as having been deposited by mass-wasting or flood events. Areas where the distinction of events using the Rb/Sr-method agrees with visual and sedimentological interpretations are shown as black bars above the core sections. Dark grey bars are suggested as events by the Rb/Sr data, but not by visual and sedimentological interpretations, whereas the light grey bar is interpreted as an event by visual and sedimentological interpretations but not by the Rb/Sr-ratio

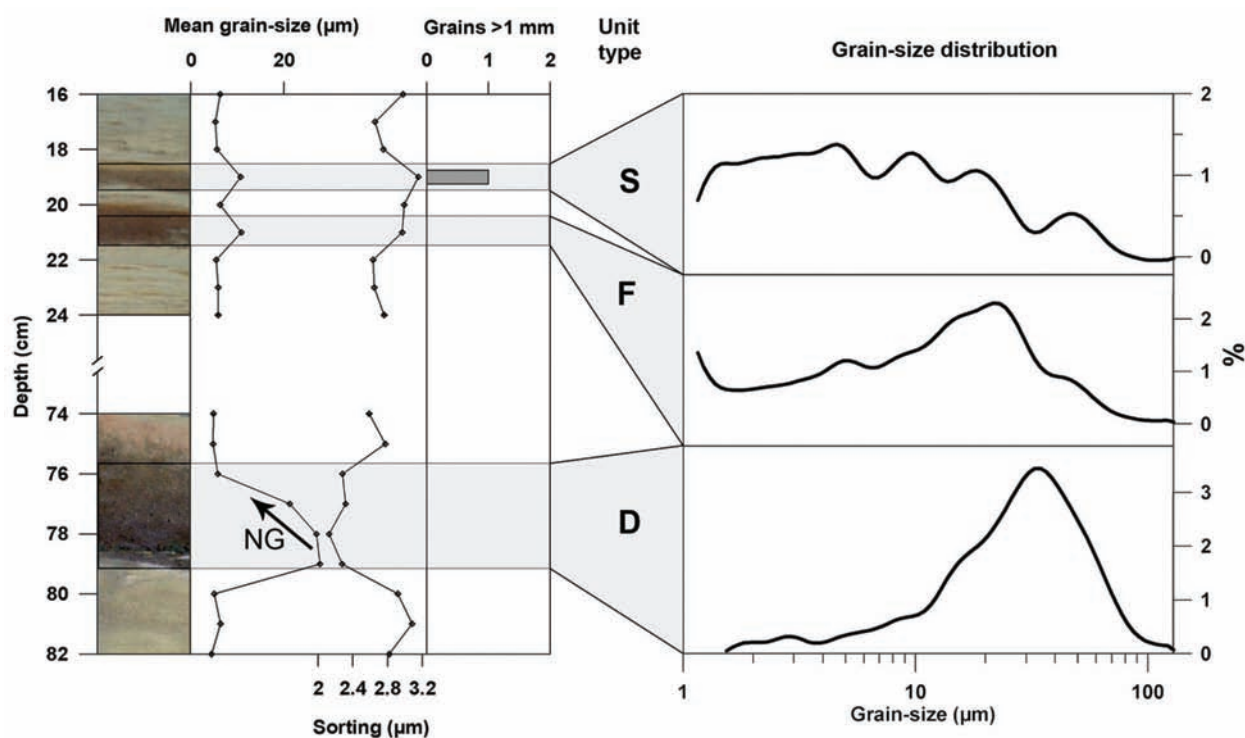


**Figure 6.** A closer look at the three different unit types found in core OLP 105. The parameters mean and sorting, the number of particles >1 mm and grain-size distributions are shown for, from the top: S-units (snow-avalanche deposits), F-units (river flood deposits) and D-units (density current deposits). NG, normal grading (fining-upwards). Note that the grain-size distribution shown for the D-unit represents the lowermost sample within that unit

hazardous events. The recognition of event layers is also critical for any further palaeoclimatic studies of the core, both because palaeoclimatic reconstructions can be severely compromised if an event layer is wrongly interpreted as a climate-driven change in sedimentation (e.g. Støren et al., 2008), and because it is necessary to recognize event layers in order to establish a reliable age–depth relationship. The distinction between event layers and background sediment is clear in the Oldevatnet cores, even macroscopically, providing an opportunity to develop and calibrate new and more objective methods for separating rapid and continuous sedimentation. This could potentially be very useful in lake studies where the difference between event layers and background sedimentation is not as obvious as in Oldevatnet. We have thus investigated the potential of bulk sediment Rb/Sr-ratio as an indicator of sediment provenance. Data from the 3.5 kHz seismic profiling, and further correlation of high-amplitude seismic reflections with event layers in the cores, also provided an opportunity to identify and determine the extent and approximate age of exceptional deposits.

### Chronology

The age–depth relationships were created using a simple linear interpolation between weighted average values of the calibrated  $^{14}\text{C}$  dates (Table 1), with event layers being treated as instantaneous deposition (Figure 7). Ages are given as calibrated years Before Present (cal. yr BP), with ‘present’ referring to AD 2000. All  $^{14}\text{C}$  dates (Table 1) were performed on terrestrial plant macrofossils, with the possible exception of a moss sample that was too degraded to properly identify (Poz-21750). Based on analysis of the seismic profiles and the relationship between dominant grain-sizes in the event layers and the background sedimentation, we postulate that no significant erosion has taken place at the OLP 105 coring site during mass-wasting or flood events. Grain-sizes in event layers recorded in OLP 105 are only rarely registering as high as the fine sand fraction, whereas the background sediment holds more than 50% clay throughout most of the core. The latter implies high cohesion in the background sediments, presumably making them resistant to erosion under the energy conditions associated with deposition of fine sand (Hjulström, 1935; Sundborg, 1956). At the more proximal OLP 305 coring site, there has most probably been erosion during some mass-wasting events. Several radiocarbon dates were performed just below and inside event layers in OLP 305 to see if the extent of erosion could be determined. Three of the dates (Poz-26485, Poz-26487 and Poz-26488) were virtually identical, most likely due to a ‘plateau’ in the  $^{14}\text{C}$  calibration curve spanning almost 400 years from about 2350 to 2750 cal. yr BP (Reimer et al., 2004). The resulting uncertainties made it impossible to determine any erosional extent using these radiocarbon ages. In the final chronology, each of these three identical dates was assigned a ‘most probable’ age based on its stratigraphic position and the probability distributions generated by OxCal (Figure 7). Most dates in core OLP 305 and a few from OLP 105 were performed on organic material retrieved from within event layers, and thus the possibility of redepositional processes had to be considered. Terrestrial macrofossils are scarce in the background sediment of Oldevatnet, yet very abundant in event layers. We therefore consider it unlikely that there is a significant contribution of terrestrial macrofossils redeposited from background sediment within any given event layer. We do not rule out, however, the possibility of redeposition of older macrofossils

from the catchment, or the possibility that large erosional events could have redeposited material from underlying event layers. The most fragile macrofossils, like leaf fragments, are less likely to survive such redepositional events and were thus preferred for dating. We interpreted one date to have been performed on redeposited material (Poz-26483), which was therefore not included in the age–depth calculations.

### Identifying event layers

**In the cores.** We propose a simple approach to elucidate sediment provenance in Oldevatnet: the sediments deposited by mass-wasting or flood events should display a lower Rb/Sr-ratio than the background sedimentation due to a higher content of chemically weathered material and a lower content of glacially derived detrital clay. Rb is commonly associated with detrital clay (Croudace et al., 2006), whereas the Rb/Sr-ratio of lake sediments has previously been used as an indicator of catchment weathering (Jin et al., 2001a, b; 2006), and to estimate weathering degree in loess-paleosol sequences in China (Chen et al., 1996, 1999). Because of similar effective ionic radii, Rb commonly substitutes for K in mineral lattices, whereas Sr commonly substitutes for Ca (Jin et al., 2006). K-bearing minerals are generally more resistant to chemical weathering than their Ca-bearing counterparts (Boggs, 2001; Jin et al., 2006), resulting in an enrichment of Ca, and thus Sr, in weathering products. Sr should thus be enriched in the material most likely to be entrained in mass-wasting events, such as pre-Holocene glaciogenic material (till), weathering material or redeposited (glacio-) fluvial material. Conversely, glaciofluvial material derived from contemporaneous glacial erosion should display higher Rb/Sr-ratios, closer to that of the source rock. It may not be possible to separate the relative contributions from weathering and detrital clay content to changes in the Rb/Sr-signal, however, the accumulated effect of the two mechanisms working in tandem provides a sensitive, high-resolution method for identifying event layers. The ITRAX-XRF-data were used to determine changes in Rb/Sr-ratio throughout the core. The ‘quality’ of the signal, or total count-rate, obtained with the ITRAX core scanner depends on several factors, such as sediment composition, water content, porosity and textural changes of the sediment (Croudace et al., 2006). Additionally, the relationship between actual count-rates obtained from different single elements is not necessarily linear in relation to the total count-rate (Croudace et al., 2006; Thomson et al., 2006). Thus, the semi-quantitative nature of the data should always be considered when interpreting ITRAX results (Croudace et al., 2006). Layers that were visually interpreted as event layers showed a generally lower total count-rate than the background sediments, suggesting that a change in Rb/Sr-ratio for these layers could simply be an artefact of a poorer overall signal. This was ruled out by running an entire core section at widely different voltage settings. Two runs were performed, with the high-voltage run resulting in Rb and Sr count-rates approximately ten times higher than the low-voltage run. The Rb/Sr-ratios resulting from the two runs showed a correlation of  $r = 0.9$  (plotted at an 11-point running mean), indicating that above a certain level this ratio is independent of the signal quality (total count-rate). A simple algorithm was employed to pick out periods where the Rb/Sr-ratio dropped below the twentieth percentile within each core section. The result indicated sections of the core representing rapid inflow of catchment-derived material, and correlated well with our sedimentological identification of event layers (Figure 5).



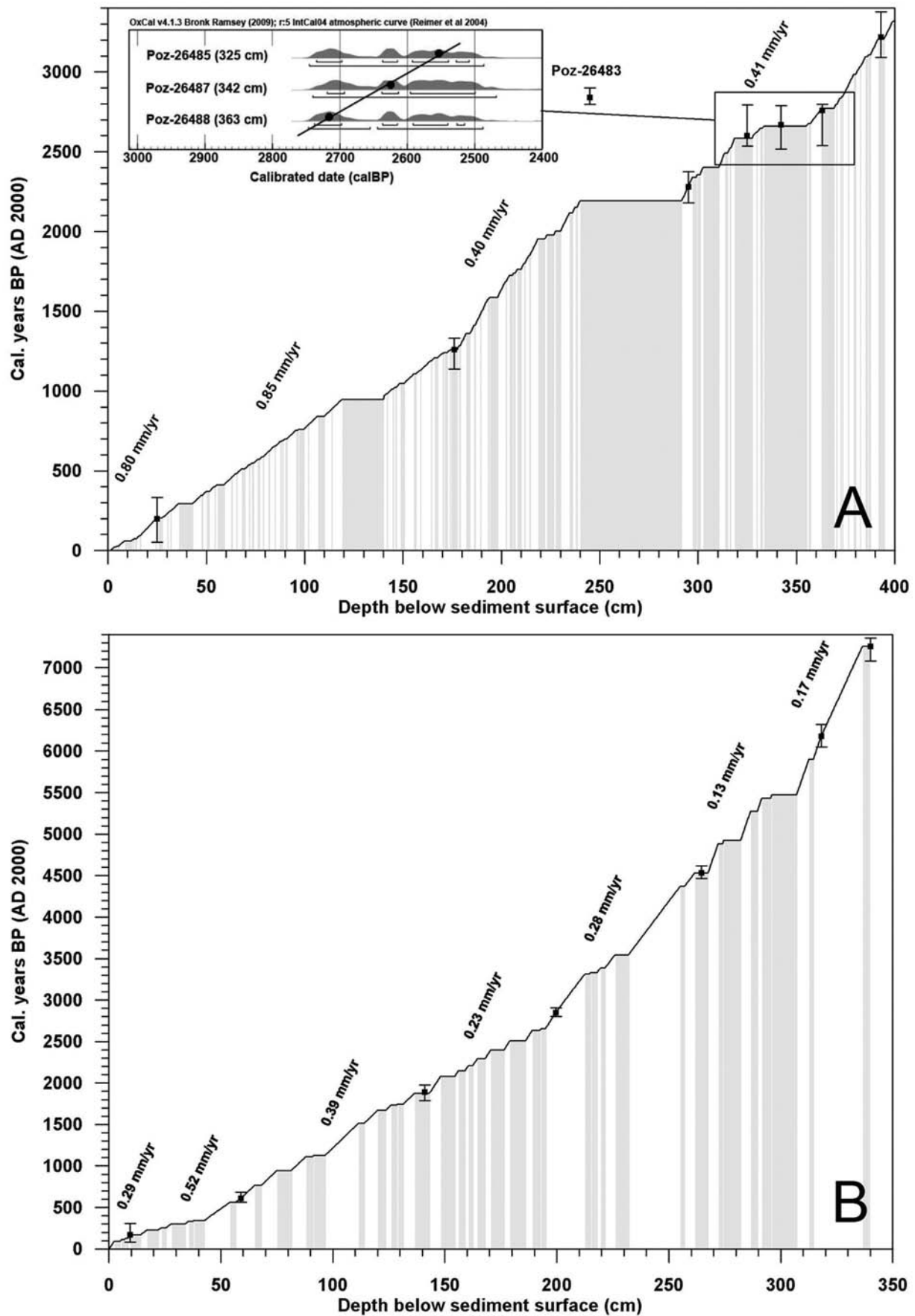


**Figure 7.** Age–depth relationships from cores OLP 305 (A) and OLP 105 (B). Event layers are shaded grey. Vertical error bars indicate two standard deviations as calculated from OxCal v4.1.3 (Bronk–Ramsey, 2009). Sedimentation rates of the background sediment were calculated using a linear interpolation and assuming instantaneous deposition of event layers. Three dates in core OLP 305 (Poz-26485, Poz-26487 and Poz-26488) were practically identical because of a ‘plateau’ in the  $^{14}\text{C}$  calibration curve (Reimer et al., 2004). The ages of these dates were interpreted according to their stratigraphic succession and their calibrated probability distributions, as shown in the inset figure (A). The date Poz-26483 was interpreted as redeposited and thereby rejected.

**In the seismic profiles.** Three high-amplitude reflections are seen at the OLP 105 site (R1, R2 and R3 in Figure 3) and correlated to thick event layers in the OLP 105 core (Figure 4). The R1 reflection occurs at *c.* 0.75 m below the lake floor (b.l.f.) and can be correlated to event 19 (Table 2) that produces a major spike in DBD between 0.77 and 0.8 m b.l.f. Similarly R2 matches DBD fluctuations related to events 38 and 39 at around 1.6 m b.l.f., whereas R3 possibly matches event 45 at *c.* 2.3 m b.l.f. Acoustic penetration ends below event 45, possibly because of the occurrence of gas in the sediment. At the OLP 305 site, reflection R<sub>a</sub> (Figure 3) at *c.* 0.5 m b.l.f. can be correlated to DBD fluctuations associated with an event layer between 0.36 and 0.45 m, whereas reflection R<sub>b</sub> matches a drop in DBD below an event layer at 1.2–1.4 m in the OLP 305 core. Below this thick event layer the acoustic signal is absorbed, in conjunction with the occurrence of hyperbolas in the seismic section. The latter suggests that the loss of acoustic signal is due to the presence of coarse-grained sediments. Age–depth relationships in the cores suggest that R1 and R<sub>b</sub> may be contemporaneous, and the possibility that these reflections represent a continuous layer deposited by the same event is discussed further below.

### Interpretation of event layers

The F-, S- and D-units (see Results) are interpreted to represent deposition from river floods, snow-avalanches and density currents, respectively. As these different types of events are related to different triggering mechanisms, it is important to distinguish between them. The differentiation was done using the grain-size properties ‘mean’ and ‘sorting’ (Blott and Pye, 2001) as well as modality. Grain-size measurements were performed on 1 cm sediment slices, and thus event layers significantly thinner than this were difficult to interpret because of the larger amount of background sediment in the sample. As a result, the interpretation of 12 layers was seen as highly uncertain (Table 2). These 12 layers all plot within the tenth to ninetieth percentile range of the background sediment values of mean and sorting (Figure 8A), reflecting the large amount of background sediment versus mass-wasting derived sediment in the related grain-size samples. The average mean and sorting values of the layers can be divided into distinct groups based on their interpretations (Figure 8A). This shows that a simple classification based on mean and sorting can be useful to separate events from background sedimentation and as a first approximation to interpret event layers.

**River flood layers (F-units).** Layers that display a single dominating grain-size mode in the coarse silt fraction are interpreted as river flood deposits (Figure 8B). The high ratio of mean particle size versus sorting, and the fining-upwards sequences that are seen in the upper part of many of the F-units, are typical for river flood layers (Arnaud et al., 2002; Bøe et al., 2006). The distinction between background sedimentation and event layers may be artificially sharp when applied to river flood events in proglacial lakes such as Oldevatnet. The bulk of annual sedimentation in a proglacial lake may in fact be the result of very short episodes of particularly high water discharge during summer melt (e.g. Østrem, 1975), and in that perspective a large percentage of the background sedimentation in core OLP 105 could be considered a product of river floods. This can be seen in many of the grain-size samples from the background sediment that display distinct modes in the silt fraction, quite similar to what is here classified as a river flood layer. Because every grain-size sample represents

between 20 to 75 years of sedimentation it is expected that each sample on average contains river flood events with recurrence intervals of up to 20–75 years. Analyzing all of these relatively high-frequency events lies outside the scope of this study, and thus they are classified as part of the background sedimentation. Only layers that are lithologically distinguishable by colour, grain-size and macrofossil content are, therefore, here defined as flood layers. This definition may seem convenient, but could also be a reflection of flood events above a certain magnitude. Frequent flooding events reduce vegetation cover in the areas where they occur, resulting in mainly redeposition of minerogenic material during subsequent events. Because there is no increase in general catchment runoff associated with floods induced by summer melt of the glaciers, these flood events will transport small amounts of terrestrial macrofossils into the lake. Extreme flood events are on the other hand able to affect more densely vegetated areas and transport considerable amounts of organic detritus into the lake. This could explain the brown colour, high LOI values and content of terrestrial macrofossils seen in the F-units of core OLP 105. Another possibility is that the macrofossil-rich flood layers represent extreme precipitation events with a high catchment runoff, resulting in deposits distinctly different from those associated with more common meltwater floods. It is more uncertain how severe events these visually distinguishable flood layers actually represent.

**Snow-avalanche layers (S-units).** The only mechanism likely to transport grains >1 mm to the OLP 105 site, is flotation by either snow or ice (e.g. Nesje et al., 2007). The presence of these coarse grains in the core could possibly be explained by a process where detrital particles from the shore are frozen within the lake ice, then rafted into deeper parts of the lake and deposited during spring melt. However, if this was a common process we should expect to find particles >1 mm in the background sediment independent of any event layers. Yet particles >1 mm were only detected within event layers, and are therefore interpreted to be connected to mass-wasting events. We consider snow-avalanches to be the most probable mechanism behind the presence of these coarse particles. A snow-avalanche is able to entrain a variable amount of minerogenic debris, dependent on its type (e.g. wet or dry), and deliver a mix of snow and debris into the lake or onto the lake ice. If the lake is not ice-covered, or the avalanche breaks the ice, very large particles will probably be deposited close to the shore, whereas gravel-size or smaller minerogenic debris will be able to float around the lake while entrained in the snow and thereby be deposited in a random fashion when the snow melts. This is one possible mechanism able to explain the scattered, coarse grains and poor sorting of the S-units in Oldevatnet. If the lake is ice-covered and the ice does not break when the avalanche hits, snow and debris will be deposited onto the ice. When the ice cover breaks during spring, the debris will be rafted along with the ice and deposited as the ice melts. This mechanism is more likely to transport larger particles into the deep parts of the lake than the abovementioned rafting by snow, and will to a higher degree concentrate the deposits downstream toward the lake outlet because of a slower melting process. While the presence of grains >1 mm is used as an indication of snow-avalanche deposition, the absence of grains >1 mm cannot by itself be used as evidence to the contrary. A distinct feature of the layers containing particles >1 mm is a strongly polymodal grain-size distribution (Figure 8B). This is interpreted as a result of the random mode of deposition



**Table 2.** Depth, thickness, grain-size parameters and inferred event types for all event layers in core OLP 105. Layers where the interpretation is considered uncertain are marked with \*

Event number	Depth in core (cm)	Thickness (mm)	Grains > 1 mm	Avg mean ( $\mu\text{m}$ )	Avg sorting ( $\mu\text{m}$ )	Inferred event
1	3.70–4.60	9	–	9.94	3.13	Snow-avalanche
2	6.95–7.30	3.5	–	7.85	3.48	Snow-avalanche
3	8.40–8.75	3.5	–	7.57	3.53	Snow-avalanche
4	9.85–10.55	7	2	7.16	3.09	Snow-avalanche
5	11.25–12.50	12.5	–	7.75	2.98	Flood
6	12.50–13.85	13.5	3	12.08	3.36	Snow-avalanche
7*	18.60–19.10	5	–	5.65	2.75	Flood
8	19.50–20.15	6.5	1	10.74	3.16	Snow-avalanche
9	20.70–22.10	14	–	10.87	2.97	Flood
10	25.30–25.55	2.5	2	5.76	2.99	Snow-avalanche
11	29.65–31.40	17.5	–	6.35	2.68	Flood
12	31.75–31.85	1	1	6.17	2.72	Snow-avalanche
13*	33.70–33.75	0.5	–	5.65	2.76	Snow-avalanche
14	36.95–37.45	5	2	8.17	2.93	Snow-avalanche
15	39.55–40.20	6.5	2	6.95	2.81	Snow-avalanche
16	42.05–42.40	3.5	–	7.15	2.75	Flood
17	55.50–56.50	10	1	5.40	2.98	Snow-avalanche
18	66.85–67.85	10	1	11.47	2.97	Snow-avalanche
19	77.15–79.90	27.5	–	20.50	2.25	Density current
20	81.5–81.55	0.5	–	6.38	3.09	Snow-avalanche
21	90.15–90.70	5.5	1	8.68	3.45	Snow-avalanche
22	94.15–95.45	13	12	6.87	3.70	Snow-avalanche
23*	95.95–96.25	3	–	4.85	2.84	Snow-avalanche
24	113.20–113.85	6.5	–	5.05	3.10	Snow-avalanche
25	121.65–123.05	14	1	5.91	3.16	Snow-avalanche
26*	127.95–128.35	4	–	4.80	2.68	Flood
27*	130.70–131.10	4	–	4.67	2.62	Flood
28	138.15–139.35	12	–	11.17	2.91	Flood
29*	140.65–140.95	3	–	5.06	2.92	Flood
30	142.25–143.00	7.5	1	6.88	3.05	Snow-avalanche
31	149.75–150.85	11	1	7.64	2.95	Snow-avalanche
32	151.95–154.20	22.5	1	9.09	3.11	Snow-avalanche
33	157.90–159.10	12	1	7.84	3.20	Snow-avalanche
34	162.05–162.50	4.5	–	8.87	3.43	Snow-avalanche
35	166.30–166.95	6.5	–	9.44	3.48	Snow-avalanche
36*	167.85–168.05	3	–	4.69	2.63	Snow-avalanche
37*	172.00–174.20	12	–	5.12	2.80	Snow-avalanche
38	174.20–176.30	21	11	15.84	3.56	Snow-avalanche
39	181.05–185.65	46	–	19.55	2.47	Density current
40	190.95–192.40	14.5	–	6.25	2.67	Flood
41*	194.50–194.80	3	–	5.19	3.01	Snow-avalanche
42	214.10–214.60	5	1	6.55	3.28	Snow-avalanche
43	217.35–217.85	5	1	6.98	3.28	Snow-avalanche
44	221.20–221.45	2.5	–	7.92	3.00	Flood
45	227.85–230.90	30.5	2	7.39	2.92	Snow-avalanche
46	231.55–232.00	4.5	–	6.02	3.27	Snow-avalanche
47*	256.60–256.90	3	–	4.86	2.82	Snow-avalanche
48	263.00–263.45	4.5	–	6.66	3.32	Snow-avalanche
49	265.45–267.40	19.5	5	6.92	3.16	Snow-avalanche
50	273.50–273.90	4	1	6.26	3.21	Snow-avalanche
51	276.10–277.05	9.5	–	6.33	3.18	Snow-avalanche
52	278.35–279.50	11.5	–	6.02	3.10	Snow-avalanche
53	280.70–281.85	11.5	–	6.64	3.33	Snow-avalanche
54	288.25–289.25	10	4	7.31	3.08	Snow-avalanche
55	293.30–295.25	19.5	2	8.68	3.41	Snow-avalanche
56	297.75–298.65	9	–	8.14	3.54	Snow-avalanche
57	300.15–301.05	9	–	5.74	3.11	Snow-avalanche
58	301.50–304.85	33.5	–	10.18	3.08	Snow-avalanche
59	305.45–306.95	15	–	6.36	3.08	Snow-avalanche
60*	314.00–314.35	3.5	–	4.90	2.92	Flood
61*	338.00–340.00	20	–	6.17	2.93	Snow-avalanche

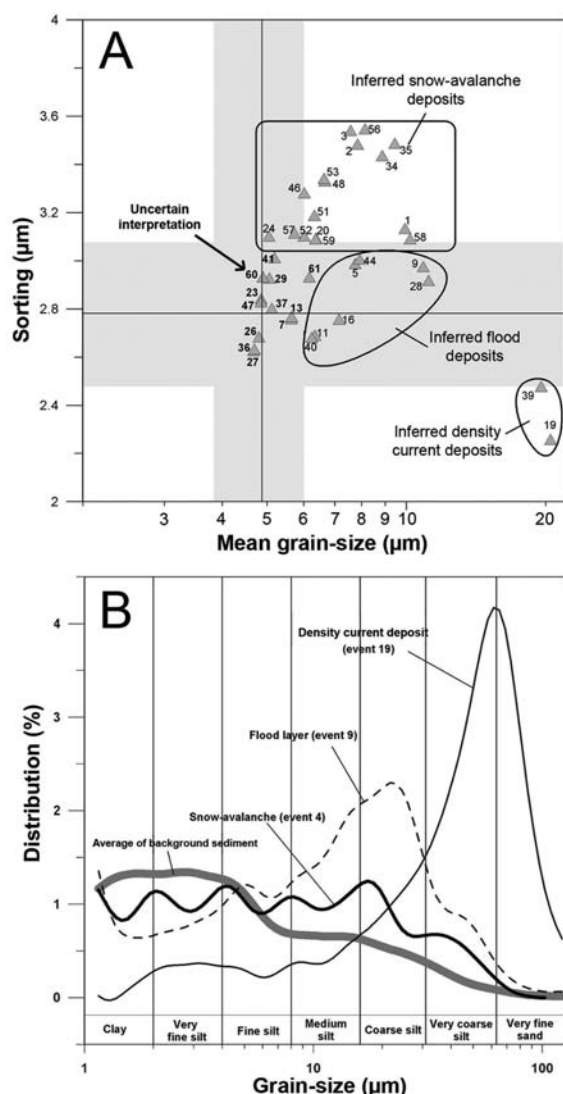


**Figure 8.** (A) Biplot showing the event layers in core OLP 105 that do not contain grains >1 mm, plotted against mean grain-size and sorting. Horizontal and vertical black lines show average values of the background sediment with grey shading indicating tenth to ninetieth percentile values. (B) The average grain-size distribution of the background sediment in OLP 105 is shown compared with typical grain-size distributions of different types of event layers

discussed above. Therefore a similar polymodal distribution is used as an indication of snow-avalanche deposition for layers that do not contain grains >1 mm as well. Ignoring the seven layers where interpretations are uncertain (Table 2), all of the inferred snow-avalanche layers feature a sorting value above the ninetieth percentile of the background sedimentation. Thus a high mean grain-size, polymodal distribution, poor sorting and presence of grains >1 mm are seen as being characteristics of snow-avalanche deposits in the OLP 105 core.

**Density current deposits (D-units).** The event layers 19 and 39 have been classified as D-units (Table 2), displaying mean and sorting values that are significantly different from all other event layers in the OLP 105 core (Figure 8A). A tentative correlation has been made between core OLP 105 and OLP 305 for these two events based on age-depth relationships (Figure 4). Event 19 has an approximate age of 950 cal. yr BP at 77–80 cm depth in OLP 105, and is correlated to a sandy, partly inverse graded layer of similar age in OLP 305 at 120–140 cm depth. Event 39 has an approximate age of 2600 cal. yr BP, and is correlated from 181 to 186 cm in OLP 105 to a gravelly layer at 335–355 cm in OLP 305. There are three distinct units within this layer in OLP 305; a 5 cm layer of massive (possibly weakly inverse graded) gravel in the basal part with particle sizes up to 6 mm, followed by a 5 cm layer of sand grading into silt, and finally a 10 cm normally graded layer consisting mostly of organic detritus. Comparable units have been identified in other lacustrine settings and interpreted as the result of subaerial debris-flows entering the lake (Sletten et al., 2003; Støren et al., 2008). An inverse grading in the basal part and normal grading in the upper part, as is most clearly seen for event 19, is a signature of hyperpycnal flood deposits associated with flash floods during extreme rainfall events (Chapron et al., 2007; Guyard et al., 2007; Mulder and Alexander, 2001). At the OLP 105 site, however, both event 19 and 39 feature a normal grading. Several possible scenarios can therefore be invoked to explain these two exceptional deposits. It is known from both marine (Meiburg and Kneller, 2010) and glaciolacustrine (Crookshanks and Gilbert, 2008) environments that turbidity currents may travel far even at very low inclinations, raising the possibility that a turbidity current induced by a subaerial debris-flow from the S2 or S5 colluvial fans (Figure 2), could be able to deposit

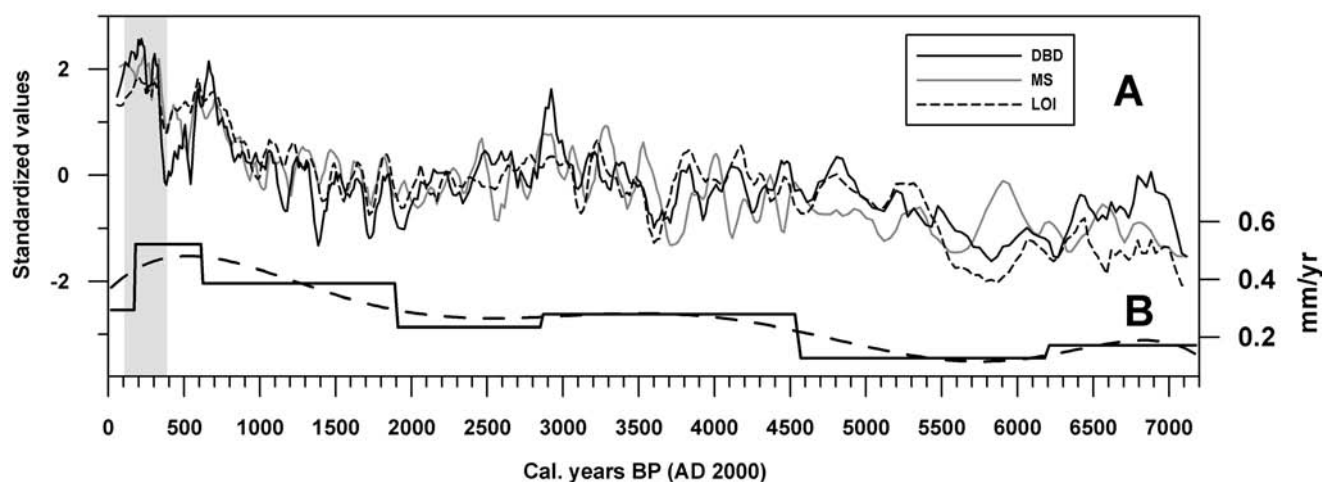


**Figure 9.** Data from the background sediment of core OLP 105. Data from event layers have been removed in order to obtain an undisturbed glacier signal. Standardized values of the physical sediment parameters LOI, DBD and MS are plotted with a five-point running mean (A). Shaded grey area show the period of maximum LIA glacier extension in southern Norway (c. 450–150 cal. yr BP; Grove, 2001). Sedimentation rate is plotted in mm/yr with a polynomial fit added as a stippled line (B)



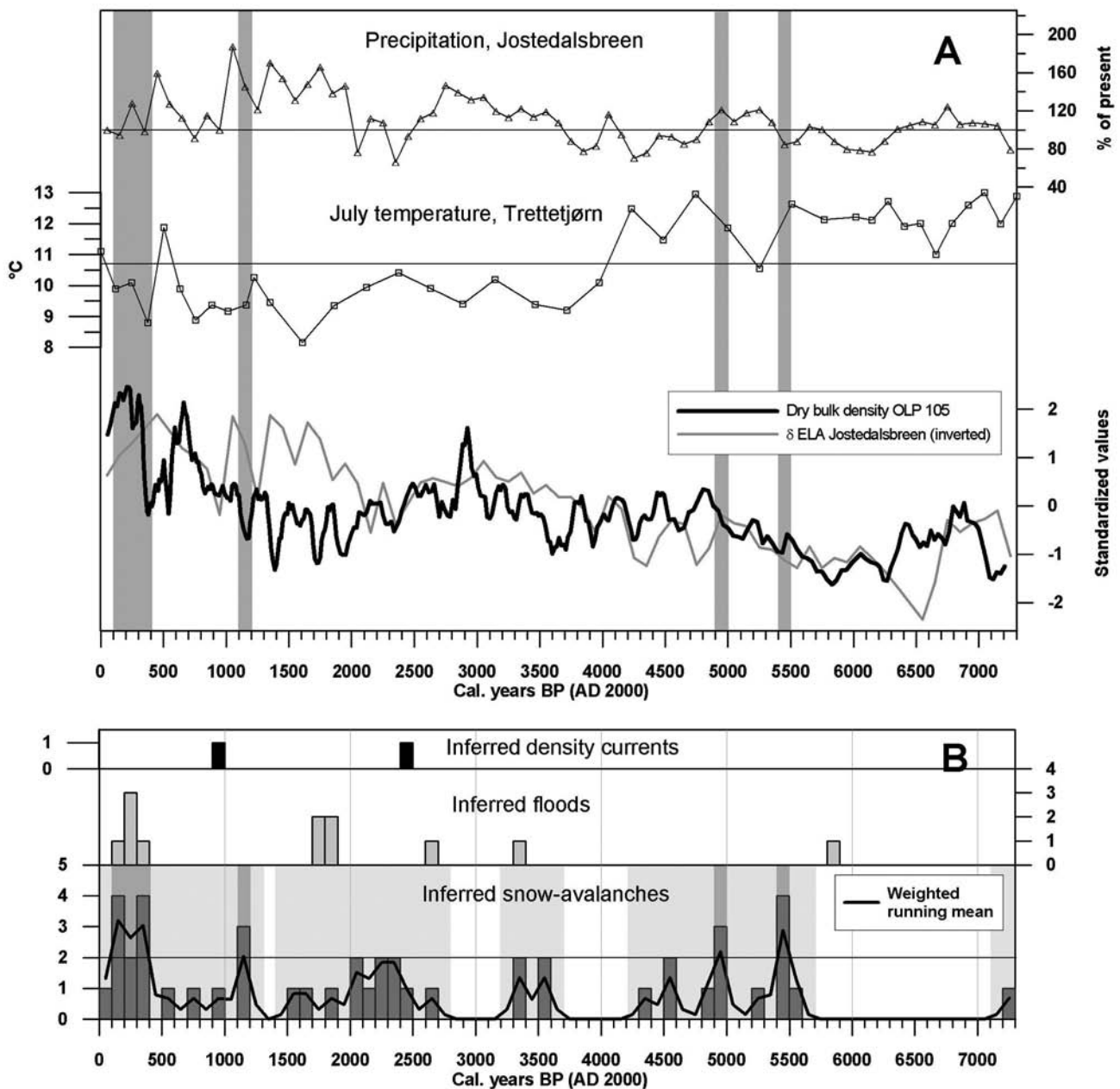


**Figure 10.** Proxy records of temperature and precipitation compared to the Oldevatnet record of mass-wasting events. (A) From the top: reconstructed winter precipitation in the Jostedalsbreen region (Bjune et al., 2005); inferred July temperature from Trettetjørn (Bjune et al., 2005); DBD record from OLP 105 compared with reconstructed ELA changes in the Jostedalsbreen region (Nesje et al., 2001b). (B) Record of density currents, floods and snow-avalanches as interpreted from the OLP 105 core. In the snow-avalanche record white areas indicate periods without large snow-avalanches, whereas light and dark grey areas indicate moderate and high frequencies of large snow-avalanches, respectively. The thick black line shows a three-point running mean, weighted with a normal distribution

fine-grained sediment and organic matter as far south as the OLP 105 site. It is uncertain whether or not the northern subaquatic ridge would work as an effective barrier able to stop a progressing turbidity current. If the deposits are the result of extreme rainfall events it is more likely that there were several different sediment sources around the lake contributing to the event layers, and at the OLP 105 site the F3 flood trajectory is a possible source (Figure 2). The seismic reflection  $R_b$  (Figure 3) is inferred to reflect event 19, and seems to be continuous north of, and possibly across, the northern subaquatic ridge. If this is correct, the R1 reflection is a continuation of the  $R_b$  reflection, and thereby supporting the turbidity current hypothesis. Neither event layer 19 nor 39 coincide with periods of inferred high earthquake activity along the coast of western Norway (Bøe et al., 2004), however, we cannot rule

out the possibility that these events were triggered by earthquakes. There is a 0.5 m thick and very chaotic unit in core OLP 305 (240–290 cm) with an approximate age of 2100 cal. yr BP that could possibly be the result of slumping triggered by the inferred high earthquake activity during this period (Bøe et al., 2004). The event layers numbered as 19 and 39 are no doubt the result of extraordinary events, but if they were related to changes in climate, extreme weather events or earthquake activity is difficult to ascertain.

#### Palaeoclimatic record

The background sedimentation is mainly the result of contemporaneous glacial erosion in the catchment with a presumably

smaller and varying contribution from redeposition through paraglacial processes (Ballantyne, 2002a, b; Church and Ryder, 1972; Støren et al., 2008). The bimodal grain-size distribution (Figure 8B) may be reflecting the sediment source, as this type of distribution is commonly seen in partially crushed and partially abraded glacial deposits (Haldorsen, 1981; Støren, 2006). In a lake setting, however, it is likely that fluvial processes are dominant in determining the final grain-size distribution of the deposited sediment. Our interpretation is that a large part of the clay and very fine silt component derive from the southern catchment area, whereas the coarser grain-sizes derive from the northern catchment area (Figure 1). Numerous studies have been conducted previously in order to reconstruct palaeoclimate and glaciation history of the Jostedalbreen region (e.g. Kvamme, 1984, 1989; Nesje et al., 2001b and references therein). The lake sediments from Oldevatnet may provide new palaeoclimatic insight by reflecting a more regional glacier signal than previous studies performed on smaller lakes in the area (Nesje et al., 2000, 2001b). This is, however, not the main focus of the present study and will be further discussed in an upcoming paper. Here we assume that the proxies LOI, DBD and MS reflect the minerogenic content of the sediments, which in turn is assumed to reflect centennial-scale glacier activity/extent in the lake catchment (Leonard, 1997). The minerogenic content (Figure 9A) shows a general rise with small oscillations from about 6000 until c. 2900 cal. yr BP, where it starts to decrease and remains low until about 1000 cal. yr BP. The highest minerogenic content in the core can be seen during the last millennium, and is probably associated with the increased glacier activity during the 'Little Ice Age' (LIA). Plotting a polynomial fit of the sedimentation rate reveals a similar pattern (Figure 9B). The overall trend in the record from Oldevatnet is in agreement with an equilibrium-line altitude (ELA) reconstruction from the Jostedalbreen region (Nesje et al., 2001b), with the exception of the ~2200 to 1000 cal. yr BP interval where the Oldevatnet record indicates a lower glacier activity (Figure 10A). Some of this difference may be due to the larger and more complex catchment area of Oldevatnet compared to lakes used in previous reconstructions (Nesje et al., 2001b). Examples of factors that could cause discrepancies include paraglacial activity and the possible presence of subglacial sediment deposits below the Jostedalbreen glacier (Burki et al., 2009).

### *The Oldevatnet snow-avalanche record*

Flood and density current deposits are not identified with sufficient frequency in the sedimentary record from Oldevatnet to be considered significant for the further discussion of this paper (Figure 10B). Being dominated by snow-avalanches, this record may therefore reflect changes in past wintertime synoptic conditions (Blikra and Selvik, 1998). From an analysis of historical data, the three most important parameters for snow-avalanche triggering in western Norway are: (1) amount of precipitation during the last day prior to the avalanche, (2) wind speed during the last day prior to the avalanche, and (3) number of positive degree days during the entire winter season (Førland et al., 2007). There are two main problems when using historical data to analyze the relationship between extreme weather events and mass-wasting activity. First, the grid of meteorological stations is not dense enough to capture local extreme weather, and second, registration of mass-wasting events is limited to incidents that cause

loss of human lives or interfere with human infrastructure (Førland et al., 2007). In this context prehistoric records have the advantage of being unbiased in relation to human activity. Although we may infer from the historical data that the snow-avalanche record presented here should to some extent reflect extreme weather events, the main challenge is to explain the centennial-scale changes seen in the record; changes that are probably a result of different climatic and meteorological mechanisms operating on highly different temporal and spatial scales.

First we need to consider what the record actually tells us. At first glance it displays periods of no apparent activity interspersed with periods of higher activity (Figure 10B). However, only snow-avalanches with the ability to entrain large amounts of sediment and transport it into the lake, or onto the lake ice, are registered at the OLP 105 site. The ability of a snow-avalanche to entrain and transport sediment is highly dependent on the snow density (Blikra and Nemec, 1998). In general, dry, powdery snow-avalanches associated with mid-winter conditions have a lower ability to transport sediment than denser, 'wet' avalanches (Blikra and Nemec, 1998). The rheology of snow-avalanches is not straightforward, however, and will not be discussed in detail here (for details see, e.g. Blikra and Nemec, 1998 and references therein). As a simplification we will define the ability to entrain and transport sediment as snow-avalanche 'size'. In this respect the Oldevatnet record only reflects the frequency of 'large' avalanches. Whether it reflects a general snow-avalanche activity is more uncertain, as this would only be the case if there is a fixed probabilistic distribution of avalanche size with respect to avalanche frequency. However, when considering the avalanche threat to the local population, the frequency of avalanches that are large enough to reach the lake are of particular interest, as most of the human infrastructure and settlements are located close to the lake shore (Figure 1).

In a record featuring centennial time resolution, uncertainties in the chronology have to be acknowledged (Table 1). Therefore a three-point running mean, weighted with a normal distribution, was applied as a simplified way of including dating uncertainty (Figure 10B). By using this approach we consider it to be 68% likely that the true age of any snow-avalanche event lies within the century that is suggested by the age-depth relationship (Figure 7), whereas it is considered as 16% likely that it lies within the preceding or following 100-year period. The record's ninetieth percentile frequency value, amounting to two events per 100 years, is used to define a significantly 'high' frequency. A high frequency of large snow-avalanches is recorded in the 5500–5400, 5000–4900, 1200–1100 and 400–100 cal. yr BP intervals, whereas periods with no large snow-avalanches occur between 7100 and 5700, 4200 and 3700, 3200 and 2800, and 1400 and 1300 cal. yr BP (Figure 10B). Periods in between the mentioned time intervals are considered to reflect a moderate frequency of large snow-avalanches.

When compared with Holocene records of July temperature (Bjune et al., 2005), precipitation and glacier variations (Nesje et al., 2001b), there are apparently no consistent connections between the snow-avalanche record from Olden and these climatic parameters (Figure 10A and B). The longest persistent period of high snow-avalanche activity, however, coincides clearly with the maximum LIA glacier extent. This is in agreement with historical documents that show an increased frequency of floods and mass-wasting events in the period between AD 1650 and 1760 (Grove, 1972; Nesje and Aa, 1989), and may

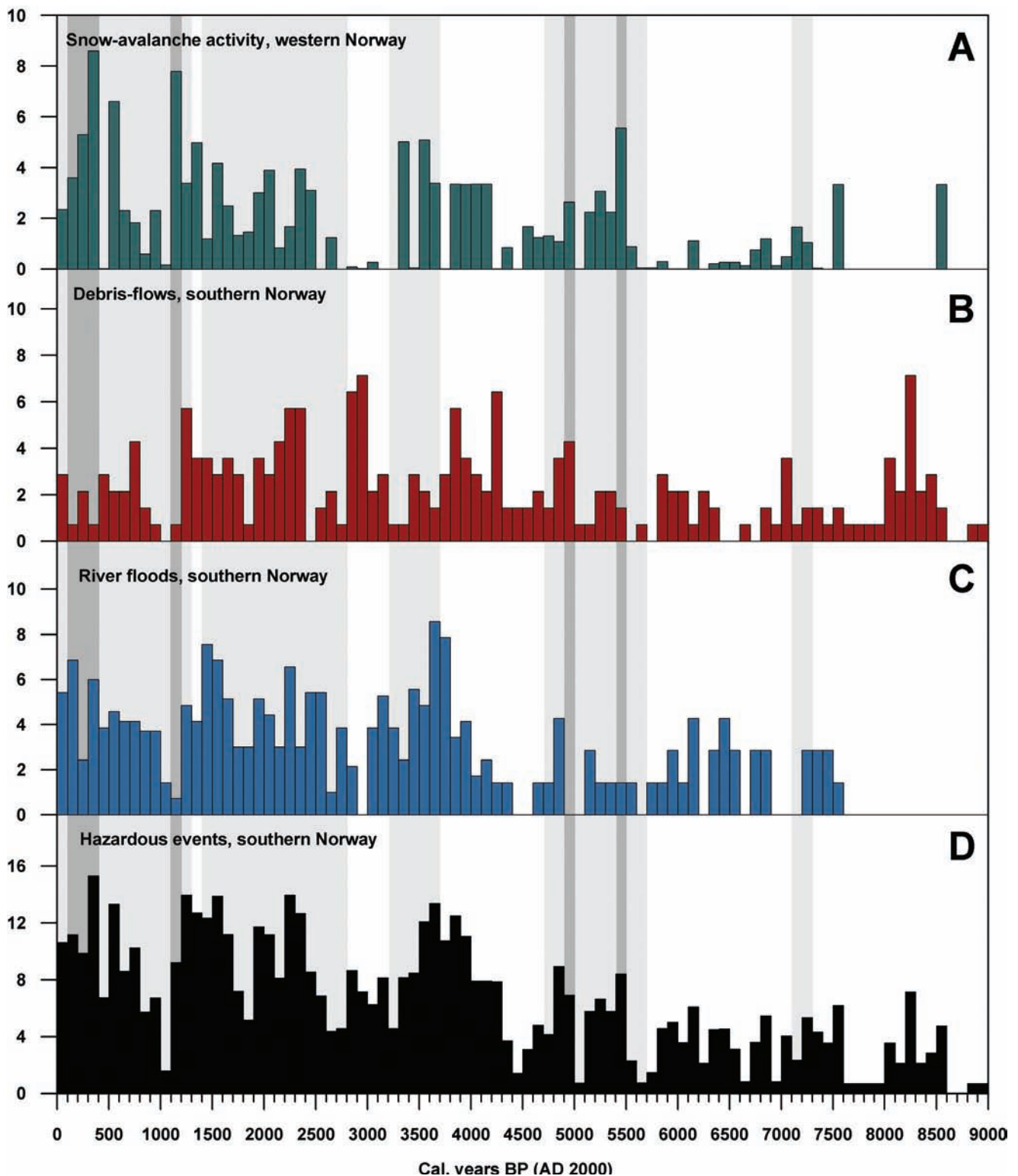


**Figure 11.** (A) Reconstructed centennial snow-avalanche activity in western Norway for the last 9000 years based on records from Møre in western Norway (Blikra and Selvik, 1998), around Vanndalsvatnet in Jostedal, western Norway (Nesje et al., 2007), and around Oldevatnet in western Norway (this study). (B) Reconstructed number of debris-flows/century during the last 9000 years based on data from Leirdalen in Jotunheimen, southern Norway (Matthews et al., 2009), and from other areas in eastern and western Norway (Blikra and Nesje, 1997; Sletten and Blikra, 2007; Sletten et al., 2003). (C) Reconstructed river floods during the last 9000 years in the catchments of the lakes Atnsjøen (Nesje et al., 2001a), Butjønna (Bøe et al., 2006) and Russvatnet (Støren et al., 2008). (D) Combined centennial snow-avalanche activity, debris-flow activity, and river flood activity for the last 9000 years in southern Norway based on the records in (A), (B), and (C). Periods of moderate and high snow-avalanche activity recorded in Oldevatnet (this study) are shaded light and dark grey, respectively

be attributed to a general increase in winter precipitation (Nesje et al., 2008). However, possible secondary effects of LIA climate on snow-avalanche frequency should not be ignored. Snow-avalanches around the northern part of Oldevatnet are

usually triggered along the fronts of local glaciers (Figure 1). It is therefore likely that the growth of these local glaciers towards the steep valley sides would cause an increased snow-avalanche hazard in itself. We therefore interpret the large increase in



snow-avalanche activity seen during the LIA to be a result of direct climatic effects (e.g. a general increase in winter precipitation) combined with the growth of local glaciers, which in turn may be considered an indirect climatic effect on snow-avalanche frequency.

### *Holocene mass-wasting and flood activity in southern Norway*

An overview of hazardous events in southern Norway over the last 9000 years is given in Figure 11 by combining several records of snow-avalanches (Blikra and Selvik, 1998; Nesje et al., 2007; this study), debris-flows (Blikra and Nesje, 1997; Matthews et al., 2009; Sletten and Blikra, 2007; Sletten et al., 2003) and floods (Bøe et al., 2006; Nesje et al., 2001a; Sletten et al., 2003; Støren et al., 2008) (Figure 11). Each record was first rescaled to a scale of 0–10 by multiplying the values with 10 and dividing by the maximum value of the record. Composite records of snow-avalanche-, debris-flow- and flood activity (Figure 11A, B and C, respectively) were then created by adding the records of the different event-types together. The number of records increases towards the present, making it necessary to divide by the number of records used within each 100 year interval. While this simple method does take some measure to avoid that single records dominate, it is impossible to avoid some bias for periods where there are very few records. Finally the snow-avalanches, debris-flows and river floods were combined to a single record indicating overall mass-wasting and flood activity in southern Norway (Figure 11D). This final composite record shows a generally increasing activity on a multimillennial scale through the Holocene, possibly reflecting long-term changes in orbital forcing. On centennial timescales the relationship between climate change and hazardous events appear far more complex, however. The seemingly periodic or quasi-periodic occurrences of events seen in the composite record (Figure 11D) show no obvious correlations with centennial fluctuations in summer temperature or winter precipitation (Figure 10A). Triggering of a single flood or mass-wasting event may result from a combination of mechanisms operating on different temporal and spatial scales, whereas the triggering causes of similar types of events may also vary between localities of different climatic regimes, e.g. between eastern and western Norway (Sandersen, 1997). Although this makes it challenging to infer the contribution of climate change in any single record of hazardous events, the possibility to identify and isolate related climate signals increases with the number of records from any specific area or region. Furthermore, if representative records from regions of different climatic regimes are analyzed and systematically compared, spatial and temporal distributions related to variations in different climatic parameters (e.g. atmospheric circulation patterns) may appear (Bøe et al., 2006; Støren et al., unpublished data, 2010). Continued study is therefore required in this field, as a denser network of Holocene event records will serve to increase our understanding of the relationship between climate and hazardous events.

## Summary and conclusions

- Two lacustrine sediment cores from the northern Oldevatnet basin have been investigated in order to reconstruct a history of hazardous events and climate change during the past 7300 years.
- Event layers were separated from background sedimentation by applying a new method related to bulk sediment Rb/Sr-ratio. Results from this novel approach are largely consistent with sedimentological evidence.
- Event layers were further differentiated using mainly grain-size data. Deposition of grains >1 mm at a distance of more than 500 m from the nearest colluvial fan were interpreted as a result of snow-avalanche deposition. Inferred snow-avalanche events dominate the record, whereas the frequencies of inferred river floods and density currents are regarded as too low to give any meaningful information related to climate.
- Periods of enhanced snow-avalanche activity are recorded at 5500–5400, 5000–4900, 1200–1100 cal. yr BP and during the LIA glacier maximum (c. 400–100 cal. yr BP). Periods without any large snow-avalanches are seen between 7100 and 5700, 4200 and 3700, 3200 and 2800, and 1400 and 1300 cal. yr BP separated by intervals of moderate activity.
- The change from moderate to high snow-avalanche activity at 400 cal. yr BP is interpreted as the result of local glacier growth related to the LIA in addition to any direct climatic effects. Glacier growth is in this respect seen as an indirect climatic effect.
- A warmer climate towards the end of the twenty-first century implies a general decrease in glacier size, something that could possibly serve to reduce snow-avalanche activity on a local scale around Oldvatnet. However, changes in conditions that are not readily inferred from palaeodata, such as wind speed and direction, may also affect future snow-avalanche activity.

## Acknowledgements

The authors would like to sincerely thank Bjørn Christian Kvisvik and Jostein Bakke for collecting the cores, Siv Tone Bårdsnes for doing part of the LOI measurements, and Anne Bjune, Ingelinn Aarnes and Hilary Birks for their help in identifying plant macrofossils for radiocarbon dating. We would also like to thank the Bjerknes Centre for Climate Research for financial support through the NORLAK project. The authors extend their thanks to John Matthews and an anonymous reviewer for valuable comments on the manuscript. This is publication no. A300 from the Bjerknes Centre for Climate Research.

## References

- Alfsnes E and Førland EJ (2006) Trends in extreme precipitation and return values in Norway 1900–2004. *met.no Report 2/2006 Climate*.
- Arnaud F, Lignier V, Revel M, Desmet M, Beck C, Pourchet M et al. (2002) Flood and earthquake disturbance of Pb-210 geochronology (Lake Anterne, NW Alps). *Terra Nova* 14: 225–232.
- Bakke J, Dahl SO and Nesje A (2005a) Lateglacial and early Holocene palaeoclimatic reconstruction based on glacier fluctuations and equilibrium-line altitudes at northern Folgefonna, Hardanger, western Norway. *Journal of Quaternary Science* 20: 179–198.
- Bakke J, Dahl SO, Paasche Ø, Løvlie R and Nesje A (2005b) Glacier fluctuations, equilibrium-line altitudes and palaeoclimate in Lyngen, northern Norway, during the Lateglacial and Holocene. *The Holocene* 15: 518–540.
- Bakke J, Lie Ø, Nesje A, Dahl SO and Paasche Ø (2005c) Utilizing physical sediment variability in glacier-fed lakes for continuous glacier reconstructions during the Holocene, northern Folgefonna, western Norway. *The Holocene* 15: 161–176.

- Ballantyne CK (2002a) A general model of paraglacial landscape response. *The Holocene* 12: 371–376.
- Ballantyne CK (2002b) Paraglacial geomorphology. *Quaternary Science Reviews* 21: 1935–2017.
- Beierle BD, Lamoureux SF, Cockburn JMH and Spooner I (2002) A new method for visualizing sediment particle size distributions. *Journal of Paleolimnology* 27: 279–283.
- Benestad RE (2007) Novel methods for inferring future changes in extreme rainfall over Northern Europe. *Climate Research* 34: 195–210.
- Birks HH and Lotter AF (2000) NORPEC sampling protocol for AMS radiocarbon dating. Unpublished protocol, NORPEC project.
- Bjune AE, Bakke J, Nesje A and Birks HJB (2005) Holocene mean July temperature and winter precipitation in western Norway inferred from palynological and glaciological lake-sediment proxies. *The Holocene* 15: 177–189.
- Blikra LH and Nemec W (1998) Postglacial colluvium in western Norway: Depositional processes, facies and palaeoclimatic record. *Sedimentology* 45: 909–959.
- Blikra LH and Nesje A (1997) Holocene avalanche history in Western Norway: Chronostratigraphy and palaeoclimatic implication. *Paläoklimaforschung* 19: 299–312.
- Blikra LH and Selvik SF (1998) Climatic signals recorded in snow avalanche-dominated colluvium in western Norway: Depositional facies successions and pollen records. *The Holocene* 8: 631–658.
- Blott SJ and Pye K (2001) GRADISTAT: A grain size distribution and statistics package for the analysis of unconsolidated sediments. *Earth Surface Processes and Landforms* 26: 1237–1248.
- Bøe AG, Dahl SO, Lie Ø and Nesje A (2006) Holocene river floods in the upper Glomma catchment, southern Norway: A high-resolution multiproxy record from lacustrine sediments. *The Holocene* 16: 445–455.
- Bøe R, Longva O, Lepland A, Blikra LH, Sønstegeard E, Haflidason H et al. (2004) Postglacial mass movements and their causes in fjords and lakes in western Norway. *Norwegian Journal of Geology* 84: 35–55.
- Boggs S (2001) *Principles of Sedimentology and Stratigraphy*. Third edition. New Jersey: Prentice Hall.
- Bronk-Ramsey C (2009) Bayesian analysis of radiocarbon dates. *Radiocarbon* 51: 337–360.
- Burki V, Larsen E, Fredin O and Nesje A (2009) Glacial remobilization cycles as revealed by lateral moraine sediment, Bødalsbreen glacier foreland, western Norway. *The Holocene* 19: 415–426.
- Chapron E, Juvigne E, Mulsow S, Ariztegui D, Magand O, Bertrand S et al. (2007) Recent clastic sedimentation processes in Lake Puyehue (Chilean Lake District, 40.50 degrees S). *Sedimentary Geology* 201: 365–385.
- Chen J, An ZS and Head J (1999) Variation of Rb/Sr ratios in the loess-paleosol sequences of central China during the last 130,000 years and their implications for monsoon paleoclimatology. *Quaternary Research* 51: 215–219.
- Chen J, Wang H and Lu H (1996) Behaviors of REE and other trace elements during weathering – Evidence from chemical leaching of loess and paleosol from the Luochuan section in central China. *Acta Geologica Sinica* 9: 290–302.
- Church M and Ryder JM (1972) Paraglacial sedimentation: A consideration of fluvial processes conditioned by glaciation. *Geological Society of America Bulletin* 83: 3059–3071.
- Crookshanks S and Gilbert R (2008) Continuous, diurnally fluctuating turbidity currents in Kluane Lake, Yukon Territory. *Canadian Journal of Earth Sciences* 45: 1123–1138.
- Croudace IW, Rindby A and Rothwell RG (2006) ITRAX: Description and evaluation of a new multi-function X-ray core scanner. In Rothwell RG (ed.) *New Techniques in Sediment Core Analysis*. London: Geological Society, Special Publications, 267, 193–207.
- Dean WE (1974) Determination of carbonate and organic matter in calcareous sediments and sedimentary rocks by loss on ignition – Comparison with other methods. *Journal of Sedimentary Petrology* 44: 242–248.
- Førland EJ, Alfnes E, Amundsen H, Asvall RP, Benestad R, Debernard J et al. (2007) Climate change and natural disasters in Norway – An assessment of possible future changes. *met.no Report 6/2007 Climate*.
- Grove JM (1972) The incidence of landslides, Avalanches, and floods in western Norway during the Little Ice Age. *Arctic and Alpine Research* 4: 131–138.
- Grove JM (2001) The initiation of the ‘Little Ice Age’ in regions round the North Atlantic. *Climatic Change* 48: 53–82.
- Guyard H, Chapron E, St-Onge G, Anselmetti FS, Arnaud F, Magand O et al. (2007) High-altitude varve records of abrupt environmental changes and mining activity over the last 4000 years in the Western French Alps (Lake Bramant, Grandes Rousses Massif). *Quaternary Science Reviews* 26: 2644–2660.
- Haldorsen S (1981) Grain-size distribution of subglacial till and its relation to glacial crushing and abrasion. *Boreas* 10: 91–105.
- Hanssen-Bauer I (2005) Regional temperature and precipitation series for Norway: Analyses of time-series updated to 2004. *met.no Report 15/2005 Climate*.
- Hanssen-Bauer I, Drange H, Førland EJ, Roald LA, Børsheim KY, Hisdal H et al. (2009) Klima i Norge 2100. Bakgrunnsmateriale til NOU Klimatilpassing. Norsk klimasenter, September 2009, Oslo.
- Hjulström F (1935) Thesis. Studies of the morphological activity of rivers as illustrated by the river Fyris. *Bulletin of the Geological Institute of Uppsala* 25: 221–527.
- Intergovernmental Panel on Climate Change (2007) *Climate Change 2007: The Physical Science Basis*. Solomon S, Qin D, Manning M, Chen Z, Marquis M, and Averyt KB et al. (eds) Contribution of Working Group I to the Fourth Assessment Report of the Intergovernmental Panel on Climate Change. Cambridge/New York: Cambridge University Press, 996 pp.
- Iversen T, Benestad R, Haugen JE, Kirkevåg A, Sorteberg A, and Debernard J et al (2005) Norges klima om 100 år - Usikkerheter og risiko. Available from <http://regclim.met.no/>
- Jin ZD, Cao JJ, Wu JL and Wang SM (2006) A Rb/Sr record of catchment weathering response to Holocene climate change in Inner Mongolia. *Earth Surface Processes and Landforms* 31: 285–291.
- Jin ZD, Wang SM, Shen J, Zhang EL, Ji JF and Li FC (2001a) Weak chemical weathering during the Little Ice Age recorded by lake sediments. *Science in China Series D-Earth Sciences* 44: 652–658.
- Jin ZD, Wang SM, Shen J, Zhang EL, Li FC, Ji JF et al. (2001b) Chemical weathering since the Little Ice Age recorded in lake sediments: A high-resolution proxy of past climate. *Earth Surface Processes and Landforms* 26: 775–782.
- Kaland PE (1984) Holocene shore displacement and shorelines in Hordaland, western Norway. *Boreas* 13: 203–242.
- Kronholm K and Stalsberg K (2009) Klimaendringer gir endringer i skredhøyhøgheten. *Klima 03/09*: Cicero Senter for klimaforskning.
- Kvamme M (1984) Vegetasjonshistoriske undersøkelser. In: Berge Meyer O (ed.) *Breheimen-Stryn. Konesjonsavgjørende botaniske undersøkelser*. Botanical Institute, University of Bergen Report 34, 238–275.
- Kvamme M (1989) Vegetasjonshistoriske undersøkelser i Sprongdalen. In: Odland A, Aarrestad PA and Kvamme M (eds) *Botaniske undersøkelser i forbindelse med vassdragsregulering i Jostedal, Sogn og Fjordane*. Botanical Institute, University of Bergen Report 47, 166–202.
- Leonard EM (1997) The relationship between glacial activity and sediment production: Evidence from a 4450-year varve record of neoglaciation in Hector Lake, Alberta, Canada. *Journal of Paleolimnology* 17: 319–330.

- Lie Ø, Dahl SO, Nesje A, Matthews JA and Sandvold S (2004) Holocene fluctuations of a polythermal glacier in high-alpine eastern Jotunheimen, central-southern Norway. *Quaternary Science Reviews* 23: 1925–1945.
- Lutro O and Tveten E (1996) *Geologisk kart over Norge, berggrunnskart Årdal M 1:250.000*. Map. Norges Geologiske Undersøkelse.
- Matthews JA and Karlén W (1992) Asynchronous Neoglaciation and Holocene climatic-change reconstructed from glaciolacustrine sedimentary sequences. *Geology* 20: 991–994.
- Matthews JA, Dahl SO, Dresser PQ, Berrisford MS, Lie Ø, Nesje A et al. (2009) Radiocarbon chronology of Holocene colluvial (debris-flow) events at Sletthamn, Jotunheimen, southern Norway: A window on the changing frequency of extreme climatic events and their landscape impact. *The Holocene* 19: 1107–1129.
- Matthews JA, Dahl SO, Nesje A, Berrisford MS and Andersson C (2000) Holocene glacier variations in central Jotunheimen, southern Norway based on distal glaciolacustrine sediment cores. *Quaternary Science Reviews* 19: 1625–1647.
- Meiburg E and Kneller B (2010) Turbidity currents and their deposits. *Annual Review of Fluid Mechanics* 42: 135–156.
- Mulder T and Alexander J (2001) The physical character of subaqueous sedimentary density flows and their deposits. *Sedimentology* 48: 269–299.
- Nesje A (1992) A piston corer for lacustrine and marine sediments. *Arctic and Alpine Research* 24: 257–259.
- Nesje A and Aa AR (1989) Isavsmelting og skred i Oldedalen. *Sogn og Fjordane Distriktshøgskole Skrifter* 1989: 1.
- Nesje A, Bakke J, Dahl SO, Lie Ø and Bøe AG (2007) A continuous, high-resolution 8500-yr snow-avalanche record from western Norway. *The Holocene* 17: 269–277.
- Nesje A, Dahl SO, Andersson C and Matthews JA (2000) The lacustrine sedimentary sequence in Sygneskardvatnet, western Norway: A continuous, high-resolution record of the Jostedalbreen ice cap during the Holocene. *Quaternary Science Reviews* 19: 1047–1065.
- Nesje A, Dahl SO, Matthews JA and Berrisford MS (2001a) A ~4500 yr record of river floods obtained from a sediment core in Lake Atnsjøen, eastern Norway. *Journal of Paleolimnology* 25: 329–342.
- Nesje A, Dahl S, Thun T and Nordli Ø (2008) The ‘Little Ice Age’ glacial expansion in western Scandinavia: Summer temperature or winter precipitation? *Climate Dynamics* 30: 789–801.
- Nesje A, Matthews JA, Dahl SO, Berrisford MS and Andersson C (2001b) Holocene glacier fluctuations of Flatebreen and winter-precipitation changes in the Jostedalbreen region, western Norway, based on glaciolacustrine sediment records. *The Holocene* 11: 267–280.
- Østrem G (1975) Sediment transport in meltwater streams. In: Jopling AV and McDonald BC (eds) *Glaciofluvial and Glaciolacustrine Sedimentation*. Society of Economic Paleontologists and Mineralogists, Special Publication 23, 101–122.
- Palmer TN and Räisänen J (2002) Quantifying the risk of extreme seasonal precipitation events in a changing climate. *Nature* 415: 512–514.
- Reimer PJ, Baillie MGL, Bard E, Bayliss A, Beck JW, Bertrand CJH et al. (2004) INTCAL04 terrestrial radiocarbon age calibration, 0–26 cal kyr BP. *Radiocarbon* 46: 1029–1058.
- Rye N, Nesje A, Lien R, Blikra LH, Eikenæs O, Hole PA et al. (1997) Glacial geology and deglaciation chronology of the area between inner Nordfjord and Jostedalbreen-Strynefjellet, western Norway. *Norsk Geologisk Tidsskrift* 77: 51–63.
- Sandersen F (1997) The influence of meteorological factors on the initiation of debris flows in Norway. *Paläoklimaforschung* 19: 321–332.
- Shakesby RA, Smith JG, Matthews JA, Winkler S, Dresser PQ, Bakke J et al. (2007) Reconstruction of Holocene glacier history from distal sources: Glaciofluvial stream-bank mires and a glaciolacustrine sediment core near Sota Sæter, Breheimen, southern Norway. *The Holocene* 17: 729–745.
- Sletten K and Blikra LH (2007) Holocene colluvial (debris-flow and water-flow) processes in eastern Norway: Stratigraphy, chronology and palaeoenvironmental implications. *Journal of Quaternary Science* 22: 619–635.
- Sletten K, Blikra LH, Ballantyne CK, Nesje A and Dahl SO (2003) Holocene debris flows recognized in a lacustrine sedimentary succession: Sedimentology, chronostratigraphy and cause of triggering. *The Holocene* 13: 907–920.
- Støren EN (2006) En studie av innsjøsedimenter fra Russvatn i Øst-Jotunheimen. Master thesis. Department of Geography, Bergen: University of Bergen.
- Støren EN, Dahl SO and Lie Ø (2008) Separation of late-Holocene episodic paraglacial events and glacier fluctuations in eastern Jotunheimen, central southern Norway. *The Holocene* 18: 1179–1191.
- Sundborg Å (1956) The river Klarälven. A study of fluvial processes. *Geografiska Annaler* 38: 125–316.
- Svendsen JI and Mangerud J (1987) Late Weichselian and Holocene sea-level history for a cross-section of western Norway. *Journal of Quaternary Science* 2: 113–132.
- Svendsen JI and Mangerud J (1997) Holocene glacial and climatic variations on Spitsbergen, Svalbard. *The Holocene* 7: 45–57.
- Thomson J, Croudace IW and Rothwell RG (2006) A geochemical application of the ITRAX scanner to a sediment core containing eastern Mediterranean sapropel units. In: Rothwell RG (ed.) *New Techniques in Sediment Core Analysis*. Geological Society, Special Publications, London, 267, 65–78.
- Vasskog K (2006) Holosen strandforskyvning på sørlige Bømlo. Master thesis. Department of Earth Science, Bergen: University of Bergen, 99 pp.